

Review

Carbon-Based Materials for Energy Storage Devices: Types and Characterization Techniques

Freddy Escobar-Teran ^{1,2,*} , Hubert Perrot ¹  and Ozlem Sel ¹

¹ Laboratoire Interfaces et Systèmes Electrochimiques, LISE UMR 8235, Sorbonne Université, CNRS, 4 Place Jussieu, 75005 Paris, France; hubert.perrot@sorbonne-universite.fr (H.P.); ozlem.sel@sorbonne-universite.fr (O.S.)

² Departamento de Ciencias Exactas, Universidad de las Fuerzas Armadas—ESPE, Sangolqui 171103, Ecuador

* Correspondence: fescobarteran@hotmail.com

Abstract: The urgent need for efficient energy storage devices (supercapacitors and batteries) has attracted ample interest from scientists and researchers in developing materials with excellent electrochemical properties. Electrode material based on carbon, transition metal oxides, and conducting polymers (CPs) has been used. Among these materials, carbon has gained wide attention in Electrochemical double-layer capacitors (EDLC) due to its variable morphology of pores and structural properties as well as its remarkable electrical and mechanical properties. In this context, the present review article summarizes the history of supercapacitors and the basic function of these devices, the type of carbon electrode materials, and the different strategies to improve the performance of these devices. In addition, we present different approaches to studying the charging mechanism of these devices through different electrochemical techniques existing in the literature, since a deeper understanding of the interfacial charge storage mechanisms is also crucial in the elaboration and performance of the electrode material. We make a comparison of the different techniques and present their advantages and challenges. Taking these advances into account, we consider that the coupling between two methods/techniques provides a better understanding of the charge storage mechanisms in energy storage devices.

Keywords: carbon materials; supercapacitors; EQCM (Electrochemical Quartz Crystal Microbalance); EIS (Electrochemical Impedance Spectroscopy); *ac*-electrogravimetry; NMR (Nuclear Magnetic Resonance)



Citation: Escobar-Teran, F.; Perrot, H.; Sel, O. Carbon-Based Materials for Energy Storage Devices: Types and Characterization Techniques.

Physchem **2023**, *3*, 355–384. <https://doi.org/10.3390/physchem3030025>

Academic Editor: Alexander V. Eletskii

Received: 29 May 2023

Revised: 18 July 2023

Accepted: 5 September 2023

Published: 13 September 2023



Copyright: © 2023 by the authors. Licensee MDPI, Basel, Switzerland. This article is an open access article distributed under the terms and conditions of the Creative Commons Attribution (CC BY) license (<https://creativecommons.org/licenses/by/4.0/>).

1. Introduction

One of the strategies to deal with climate change is to reduce the consumption of fossil fuels and develop renewable and sustainable energy sources. In this way, more efficient electrical energy conversion and storage devices are required Kabeyi and Olanrewaju [1,2]. Batteries and supercapacitors are the most used energy storage technologies. Batteries store energy through faradaic redox reactions providing a high-energy supplement, with energy densities of a few hundreds of $W\ h\ kg^{-1}$. However, these battery-type faradaic reactions undergo slow kinetics leading to limited energy yield and lifetime [3]. In contrast, supercapacitors store the charge on reversible electroadsorption of electrolyte ions toward the surface of electrodes [4]. Although featuring lower energy density, supercapacitors can provide a high power delivery in a relatively short time and can operate for a high number of charge/discharge cycles and a longer lifetime than batteries [2,5], as shown in the Ragone Plot (Figure 1). These fast and highly reversible storage mechanisms make supercapacitors promising candidates for energy storage devices, which are presently used in a broad range of applications ranging from small devices (watches, sensors, mobile, headphones, and others) [6] to large-size cells for automotive transportation such as electric car and buses and their charging stations [7].

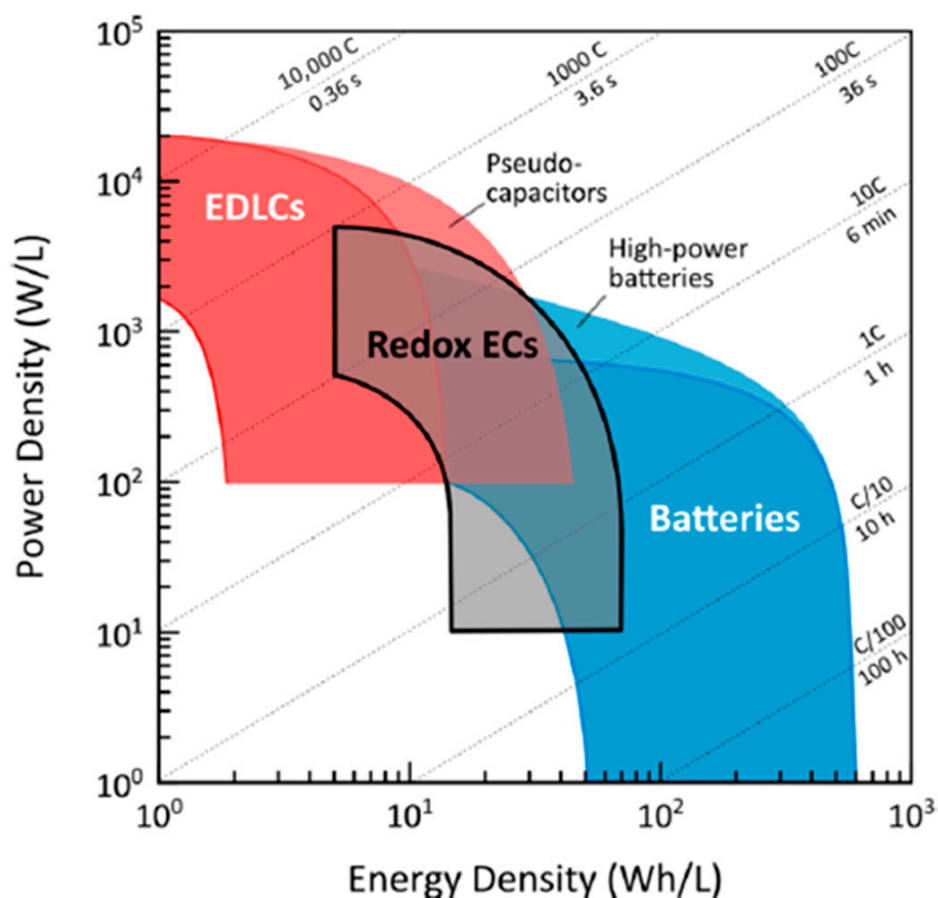


Figure 1. Ragone plot for supercapacitors and batteries. Reproduced from Ref. [8] with permission from the American Chemical Society (copyright 2017).

1.1. History

H. Becker of GEC (General Electric Company) patented the first supercapacitor in 1957. Electrodes composed of porous carbon and an aqueous electrolyte based on sulfuric acid were used by Becker. It formed an electric double layer at the electrode/electrolyte surface [9]. A few years later, a device using graphite was patented by SOHIO (Standard Oil of Ohio). In an experiment with organic electrolytes, SOHIO observed a higher operating voltage than those obtained in aqueous electrolytes. In 1971, NEC (Nippon Electric Company) licensed the SOHIO patent under the name of “supercapacitors”. NEC successfully introduced these new devices on the market as backup memories for electronics [10–12]. Following the success of NEC, several companies began to produce and develop supercapacitors. For instance, in 1982, the first high-power supercapacitor intended for military applications was designed by Pinnacle Research Institute [9,13].

Presently, there are different types of supercapacitors in terms of charge-storing mechanisms. The two main types are the Electrochemical double-layer capacitors (EDLC) and the so-called Pseudocapacitors. In EDLC, the charge is stored by electrostatic interaction between electrolyte ions and the surface of electrodes, typically using carbon materials as electrodes. In pseudocapacitors, the charge is stored by fast and reversible faradaic redox reactions between the electrolyte and electroactive species on the surface of the electrode, generally using conducting polymers (CPs) and transition metal oxide materials as electrodes [5]. Finally, another type of supercapacitor is the so-called hybrid capacitor, where the charging mechanism is due to electrostatic interactions and faradaic reactions [14] (See Figure 2).

Supercapacitors can be classified as symmetric and asymmetric. Symmetric is when both electrodes have the same design and mass loading, while in asymmetric, both electrodes are different [15].

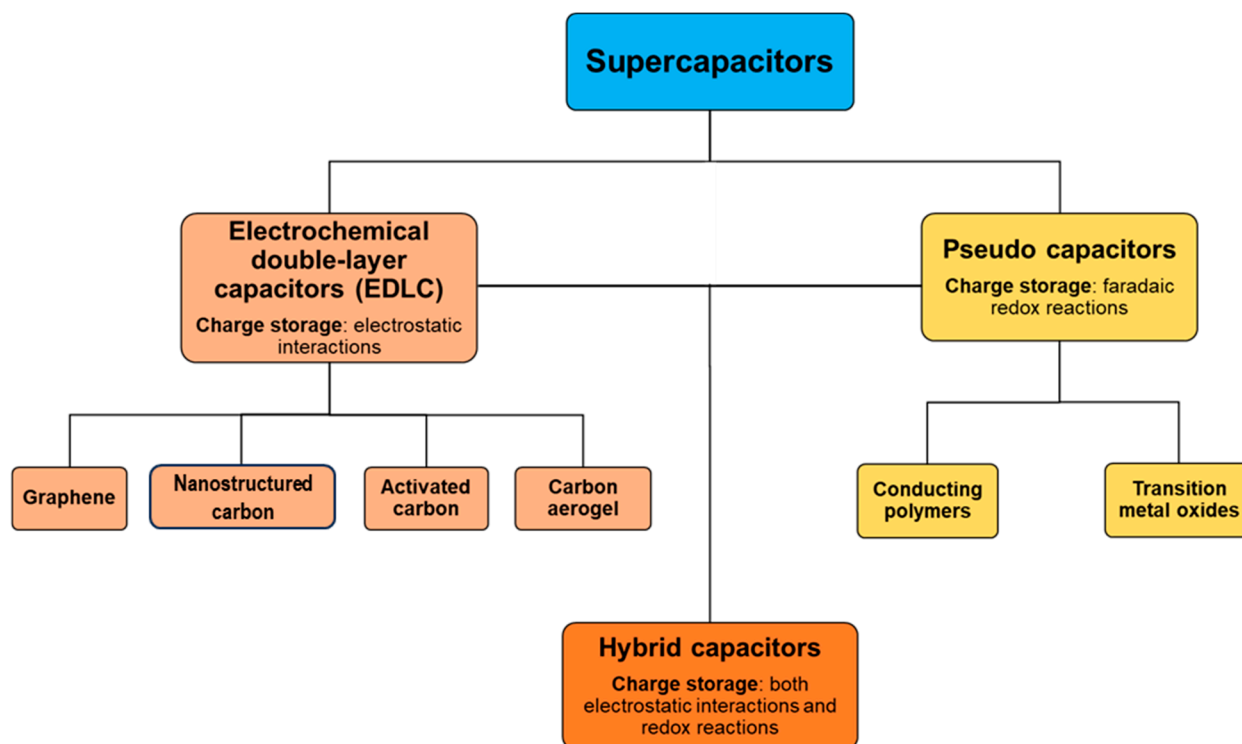


Figure 2. Categorization of supercapacitors: Electrochemical double-layer capacitors (EDLC), Pseudocapacitors and Hybrid capacitors.

1.2. Principle of Operation for EDLC

An EDLC is generally made up of two electrodes immersed in an electrolyte and insulated by a separator [12,16–18]. The two electrodes can be composed of identical or different materials. Nanostructured and porous carbons with high specific surface areas are the most commonly used [12]. The electrode materials play an important role in the capacitance values and the charge stored in the EDLC [16,17]. In EDLC, no faradaic redox reactions are involved in the electrochemical process [17]. The principle of operation is based on an electrochemical double layer. It is formed through electrostatic interactions between the electrode surface and electrolyte [12,13,16,19]. During discharge, electrical energy is generated when the accumulated charge causes a parallel movement of electrons in the external circuit, as indicated in Figure 3 [12,13]. Due to the high specific surface area of the electrode materials, the amount of energy that can be stored is much larger than in traditional capacitors [18] and the stored charge can be restored more efficiently than in batteries [20]. Furthermore, the life cycle of an EDLC is significantly higher compared to batteries. EDLCs can withstand millions of cycles [2], while batteries have a life cycle of approximately 500–2000 cycles [19]. As described above, the two electrode/electrolyte interfaces in an EDLC function as two capacitors in series (C_1 and C_2) formed at the electrode/electrolyte interfaces. Thus, the total specific capacitance of the cell (C) depends on the capacitance of each electrode. It is described in the following equation [19]:

$$\frac{1}{C} = \frac{1}{C_1} + \frac{1}{C_2} \quad (1)$$

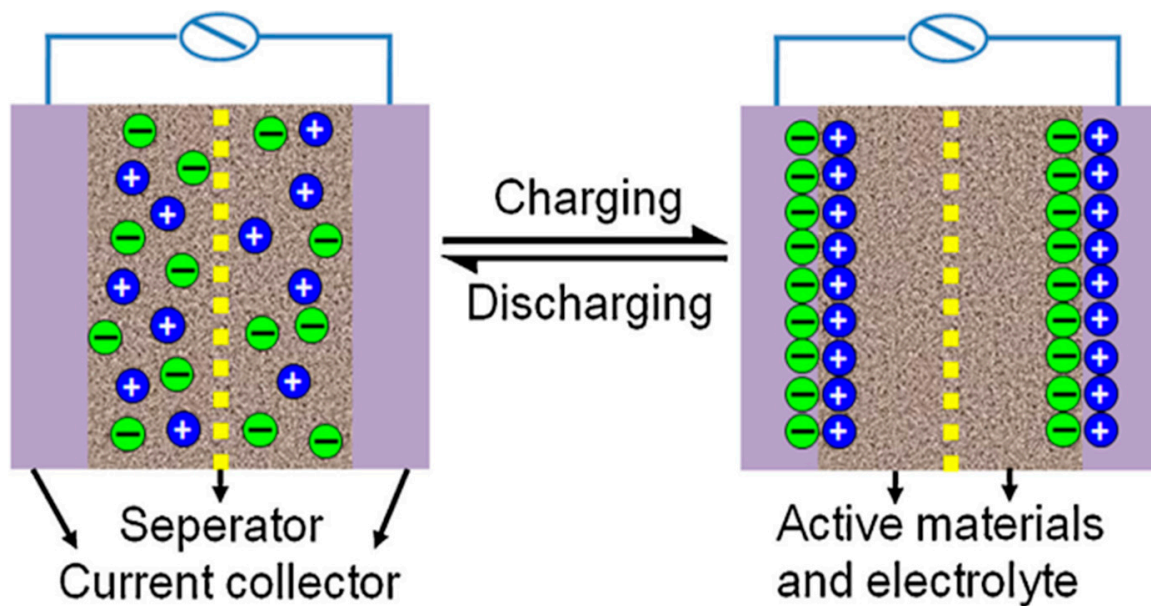


Figure 3. Charged (right) and discharged (left) states of an EDLC. Reproduced from Ref. [21] with permission from Elsevier (copyright 2013).

The relationship between the capacitance C (in Farad), the quantity of stored electrical charge Q (in Coulomb), and the rated voltage V (in Volt) is as follows [22]:

$$C = \frac{Q}{V} \quad (2)$$

where the charge Q equals the current I (in Ampere) multiplied by time t (in seconds) [12]:

$$Q = I \times t \quad (3)$$

Generally, the charge Q is expressed in Ah/g (1 Ah = 3600 C) and the specific capacitance C is given as the specific capacitance in F/cm² or F/g.

1.3. Components of the Supercapacitors: Active Electrode Materials, Electrolytes, Separator, and Current Collectors

The components of the supercapacitors are (i) active electrode materials, (ii) electrolytes, (iii) separators, and (iv) current collectors. They are detailed below.

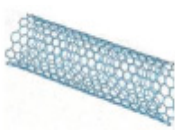
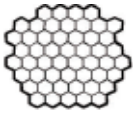
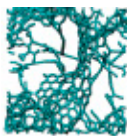
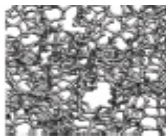
(i) Active Electrode Materials:

The main components of electrodes are the active materials. They store/deliver charges. The electrode material plays an important role in determining the capacitance, energy, and power density of the supercapacitor [23]. Moreover, it affects the series resistance and self-discharge characteristics [17,24]. Thus, the selection of the electrode materials is fundamental, and a huge number of parameters need to be considered. Such parameters are specific surface area, porosity, structure [25], “tunability” of the morphology (i.e., how readily the material allows manipulation of pore size, pore distribution, surface functional groups, etc.) [9,26], surface wettability, electrical conductivity [9], electrochemical stability [17], thermodynamic stability for a wide operational potential range, cycle stability [9], mechanical resilience [27], and cost [9,17,25]. Considering the pore size, the IUPAC (International Union of Pure and Applied Chemistry) has suggested the following classification: macropores (diameters > 50 nm), mesopores (diameters between 2 and 50 nm), and micropores (diameters < 2 nm) [28].

At the present time, there are three main categories of active electrode materials based on carbon materials [12], transition metal oxides, and conducting polymers. Among these

classes of materials, carbon is the most frequently used in EDLCs [25], and the various structures of carbon can affect their properties. The most commonly used structures in EDLCs are: (1) onion-like carbons (OLCs), (2) carbon nanotubes (CNTs), (3) graphene, (4) carbide-derived carbons (CDCs), (5) activated carbons (ACs), and (6) templated carbons (See Table 1) [16,29].

Table 1. Carbon structures with some of their characteristics. Reproduced from Ref. [30] with permission from the American Chemical Society (copyright 2013).

Material	Carbon Onions	Carbon Nanotubes	Graphene	Activated Carbon	Carbide Derived Carbon	Templated Carbon
Dimensionality	0-D	1-D	2-D	3-D	3-D	3-D
Conductivity	High	High	High	Low	Moderate	Low
Volumetric Capacitance	Low	Low	Moderate	High	High	Low
Cost	High	High	Moderate	Low	Moderate	High
Structure						

(1) Onion-Like Carbons (OLCs)

OLCs are zero-dimensional (0D) materials [30,31] that involve concentric graphitic shells with a specific surface area. The surface areas range from 200 to 980 m²/g depending on the synthesis conditions. Annealing of nanodiamond powders in a vacuum or under argon is generally the OLC preparation method [30]. They offer high electrical conductivity [30], high power [30], and high energy densities. However, a limited capacitance of around 30 F·g⁻¹ is found in these kinds of materials [30].

(2) Carbon Nanotubes (CNTs)

Multi-walled carbon nanotubes (MWCNTs) were first discovered by Sumio Iijima in 1991, as soot-like products in the Krätschmer–Huffman arc discharge synthesis reactor used for the formation of fullerene (C₆₀), and reported the existence of single-walled carbon nanotubes (SWCNTs) two years later [10,32]. CNTs are considered one-dimensional since the graphite walls that compose them are assembled in almost one-dimensional tubes and charge transport only occurs along the axis of the tube [9]. The *sp*² hybridization and the interplanar distance of 0.335 nm in the hexagonal atomic lattice remain the same in CNTs as in graphite [33]. The diameters of these tubes are approximately 1–50 nm. Depending on the number of graphitic layers (walls), CNTs are divided into three sub-groups: single-walled nanotubes (SWNTs), double-walled nanotubes, and multi-walled nanotubes (MWNTs) [18,27]. Both SWNTs and MWNTs are appreciated for their high electrical conductivity [18,27], unique pore structure [34], excellent mechanical properties [9,34], chemical reactivity [34], and thermal stability [27], and relatively low equivalent series resistance (ESR) (lower than activated carbon) [29]. Although their surface area is relatively moderate compared to activated carbon, it can be used more efficiently because the mesopores are interconnected, providing access to almost all of the surface area and allowing continuous charge distribution [27,29,34]. Taken together, these properties make CNTs suitable for high-power devices [18,27,29]. The specific capacitance of CNT electrode material varies between 15 and 200 F·g⁻¹. However, it depends on the morphology and purity obtained during the production procedure and any subsequent treatment [9,27]. Three major methods can be used to produce CNTs in sizeable quantities: arc discharge, laser ablation, and chemical vapor deposition (CVD) [35–37]. Each of these methods has advantages and disadvantages that result in different growth results (See Table 2).

Table 2. Summary and comparison of synthesis methods of CNTs. Adapted from Ref. [38], open access.

Method	Arc-Discharge	Laser-Ablation	CVD
How	CNT growth on graphite electrodes during direct current arc-discharge evaporation of carbon in presence of an inert gas [39].	To form CNTs, the vaporization of a mixture of carbon (graphite) and transition metals located in a target is used [40].	Fixed bed method: decomposition of acetylene on graphite support iron particles at 700 °C [41].
Yield rate	>75%	>75%	>75%
SWCNT or MWCNT	Both	Both	Both
Advantage	Simple, inexpensive, high-quality nanotubes.	Relatively high purity CNTs, room-temperature synthesis.	Simple, inexpensive, low temperature, high purity, large-scale production, aligned growth is possible.
Disadvantage	Purification of crude product is required, the method cannot be scaled, it must have a high temperature.	Method limited to the lab scale; crude product purification required.	Synthesized CNTs are usually MWNs, defects.

Therefore, the choice of the method depends on the requested properties of the CNTs. Prasek, J. et al. [42] reported that the choice of catalyst is one of the most important parameters when using the CVD method because it affects the CNT growth. Moreover, CNT production (CNT growth) depends on the processing conditions, such as temperature and pressure. Temperatures greater than 900 °C result in SWCNTs, while MWCNTs are formed at temperatures in the range of 700–800 °C [43].

(3) Graphene

Graphene is another active material commonly used in energy-storage mechanisms. The graphene material can host ions (such as Li⁺ or Na⁺ in metal-ion batteries) to store electrostatic charges on the electrode double layer (as in EDLC applications) [44].

Graphene is composed of pure carbon organized in a hexagonal structure in the form of a transparent sheet one atom thick. Graphene can be produced by mechanically exfoliating graphite (which is made up of interleaved sheets of graphene) with a Scotch tape method. This approach involves removing a piece of graphite until only one layer remains. However, this technique does not allow large-scale production of graphene, and since most chemical and electrochemical energy storage systems require large amounts of graphene, many other methods have been proposed to synthesize graphene-like materials. For example, graphene oxide (GO) reduction can be used to make graphene-like materials. GO is usually synthesized through the Hummers method [45], which is a reaction implying graphite, sulfuric acid, and potassium permanganate. Once the GO is synthesized, its reduction can be performed in three different manners: chemically, thermally, or electrochemically. The reduction process has a decisive influence, as it determines the quality of the reduced graphene-like material [46]. Many approaches to chemical reduction can be performed in order to bring the GO structures as close as possible to those of graphene obtained by the Scotch Tape method. Hydrazine is involved in the most common method. This compound is interesting because, unlike other reducing species such as lithium aluminum hydride (LiAlH₄), it does not react with water, thus avoiding a series of secondary reactions. However, a large-scale production implicating hydrazine would be difficult as this compound is toxic and cannot be used in the context of sustainable development. Another method involved in the production of graphene-like material is thermal reduction, which can be carried out by heat-treating graphene oxide at 1050 °C. Total elimination of carbonyl groups by thermal reduction is possible at a very high temperature (>1000 °C) and low pressure [47]. This thermal process leads to an increase in the pressure within the material because this process causes the liberation of bound oxygen in the form of CO and CO₂ [48]. However, thermal treatment of graphene oxide may cause damage to the material, causing surface defects that affect electronic properties. Nevertheless, this ecological method avoids the use of dangerous species such as hydrazine and allows the production of high-quality graphene-like material [46].

An environmentally friendly method is electrochemical reduction. In this method, a reaction in an electrolyte is carried out in a three-electrode system with a working electrode

on which GO thin films are deposited and is generally used to apply a negative voltage to produce RGO (Reduced Graphene Oxide) through a reduction reaction. The brown color of GO is modified to black when RGO is formed [49]. In some experiments, Electrochemically Reduced Graphene Oxide (ERGO) can be obtained by chronoamperometry at -1.1 V vs. Ag/AgCl for 30 min [50].

(4) Carbide-Derived Carbons (CDCs)

The carbide precursors obtained from the extraction of metals at high temperatures are used for the manufacture of CDC [30]. The porosity is formed by leaching out metal atoms from the crystal structure of the carbide precursor [30]. Furthermore, the pore structure is highly dependent on the carbide precursor and the synthesis temperature [51]. Carbon growth can be controlled on the atomic level, leading to a highly controllable pore size with better than angstrom accuracy. The specific surface area ranges from 1000 to 3000 $\text{m}^2\cdot\text{g}^{-1}$.

(5) Activated Carbons (ACs)

The carbonization of carbonaceous organic precursors (e.g., nut shells, wood, peat, or coal) [30,31,52] is generally used to produce ACs and subsequent activation processes [30,31,52]. A three-dimensional porous network in the bulk of the carbon material can be created through the activation of processes [52]. These processes can be physical and/or chemical [30]. In physical activation, an oxidizing gas [31,52], e.g., air [31,52], water vapor, CO_2 [30,31,52], or KOH [30], is used for the thermal treatment of the carbon precursor. Chemical activation is executed through an activating agent, e.g., phosphoric acid, potassium hydroxide, sodium hydroxide, or zinc chloride (H_3PO_4 , KOH, NaOH, ZnCl_2) [30,31,52]. Throughout the activation processes, micropores and mesopores can be created and the specific surface area can exceed 2000 $\text{m}^2\cdot\text{g}^{-1}$ [30]. However, the control over porosity is limited, resulting in a broad pore size distribution, which means that not all pores will be accessible to ions. AC materials with different functional groups on the carbon surface may be obtained by selecting the carbon precursor, activation method, and control of synthesis conditions. In this way, a variety of physicochemical properties can be achieved [31,52]. Functional groups containing oxygen and/or nitrogen are the most common [31].

In the last decade, the capacitive performance of ACs has been significantly improved and ACs have a higher energy density than CNTs and graphene (AC volumetric capacitance reaches 50–80 $\text{F}\cdot\text{cm}^{-3}$) [30]. ACs are widely used in commercial EDLCs [30,52] as manufacturing is scalable and the cost is reasonable.

(6) Templated carbons

The carbonization of a carbon precursor in nanochannels of a template inorganic material and the subsequent removal of the template are used to produce templated carbons [30,31,34,51,52]. Porous carbons with different physical and chemical properties may be obtained through the selection of carbon precursor and template, and by controlling the carbonization parameters [31]. The preparation of 1D, 2D, and 3D carbons, e.g., carbon nanotubes, graphene, and nanoporous carbons, can be obtained by using the template method [30], and both microporous and mesoporous carbons can be formed [51]. Furthermore, the precise control of pore structure can be achieved by this method. In this way, pore volume [51] and pore size [30] can be controlled by tuning the pore size of the template [34]. According to the templates used, it can be subdivided into hard-template and soft-template methods. A replication synthesis with pre-synthesized hard templates (inorganic materials such as silica nanoparticles, zeolites, mesoporous silica, and MgO) including infiltration, carbonization, and removal of templates is involved in the former [34], while the latter uses triblock copolymers as the template [30,34] and includes condensation and carbonization. Large-scale production is unsuitable for the hard-template method because it is expensive and time-consuming. In addition, toxic acids are required to remove the template. The soft-template method is faster, less expensive, and more ecological [34]. Templated carbons are suitable to study the effects of pore size, pore shape, and channel structures due to their

controllability. Parameters related to ion diffusion and charge storage in nano-confined systems are also analyzed [31].

In addition to carbon structures, the porous texture plays an important role in understanding the relationship between the specific surface area and the capacitance. A strong impact on capacitance values can occur through the ion size/pore size and the connection between the pores, particularly when high current densities operate in supercapacitor materials. Four important porous characteristics for carbon materials are presented: (a) ion sieving, (b) ion desolvation, (c) pore saturation, and (d) distortion.

a. Ion Sieving

Aurbach et al. [53] defined the concept of ion sieving, and it denotes the possibility of selective electrosorption of ions based on size [54–56]. The sieving effect was demonstrated in a study of the capacitance of active carbon (AC) in a series of ILs (Ionic Liquids) of increasing cation size. Since ILs are solvent-free, the capacitance properties can be interpreted by comparing the size of pores and ions calculated by molecular modeling. This study showed an extensive mismatch between the pore size and the effective size of the cations [25].

b. Ion Desolvation

Due to the solvation shell, the effective ion size in aqueous and organic electrolytes is larger than the actual ion size itself. Solvation shells are formed surrounding the ions in aqueous and organic electrolytes [25]. Therefore, the effective ion size is larger than the actual ion size itself. Although it is clear that pore size and effective ion size need to correspond, it is difficult to identify the optimal pore size, i.e., the pore size leading to the best EDLC performance. For templated carbons measured by CO₂ gas sorption, Vix-Guterl et al. [57] showed that the capacitance is proportional to the ultra-micropore volume (pores smaller than 0.7–0.8 nm), in both aqueous and organic media. Furthermore, it was shown that the ions needed to be at least partially desolvated to access the pores (for a two-electrode setup).

c. Pore Saturation

It was shown by Mysyk et al. [58] that the porosity of carbons with subnanometer-sized pores (pitch-derived carbon (PC)) can be saturated with electrolyte ions for high voltage values in a 1.5 M TEA-BF₄/ACN electrolyte. Furthermore, it was found that the capacitive current decreased significantly at a voltage above 1.5 V, although the pore size probably matched the ion size. The charge was approximately equal to the theoretical maximum charge storable in the pores larger than the desolvated cations. Therefore, the authors proposed that saturation of the ion-accessible pore volume caused a decrease in capacitive current.

d. Distortion

In a study conducted by Ania et al. [59], an unexpectedly high capacitance (92 F/g) for a microporous carbon in TEA-BF₄/ACN electrolyte was observed, where 63% of the pores were smaller than the desolvated ion size. The authors proposed that distorted cations penetrate the pores under the effect of the electric field, proving slightly smaller dimensions than their computed rigid size. A size smaller than the average pore size of carbon has been computed for some TEA⁺ conformations. Chmiola et al. [60] also observed an anomalous increase in carbon capacitance at pore sizes less than 1 nanometer.

In summary, Table 3 details different synthesis methods for supercapacitor electrode materials. Advantages and disadvantages are also included.

Table 3. Advantages and disadvantages of synthesis methods for electrode materials of supercapacitors. Reproduced from Ref. [61] with permission from Elsevier (copyright 2014).

Method	Morphology	Advantages	Disadvantages
Electrochemical deposition	Nanostructured film	Less time required; morphology can be controlled through the control of synthesis parameters such as time, temperature, etc.	Unsuitable for large-scale production
Hydrothermal method	Nanostructured film and powder	Large-scale production, easy control of morphology	High-temperature and time-consuming operations
Chemical bath deposition (CBD)	Nanostructured film	Faster than hydrothermal method, large-scale production, easy control of morphology	Only some metal oxide can be possible to synthesize
Sol-gel	Nanostructured film and powder	Low costs; controllable film texture, composition, homogeneity, and structural properties	Difficult to produce films with controlled porosity, needs the use of hard/soft templates
Chemical precipitation	Powders, colloidal nanostructures	Allows synthesis of composite electrode materials; efficient; easily implemented	Difficult to control morphology and may generate a waste product
Chemical Vapor Depositions (CVD)	Nanostructured film	High material yield than CBD; good film uniformity	Expensive equipment and relatively high costs

(ii) Electrolytes:

Supplying the ions to form the electrical double layer located between the electrode and the electrolyte is primarily the role of the electrolyte (which is made of a salt and a solvent) [12,25,62]. Therefore, electrolytes need to be good ionic conductors. Along with ionic conductivity, which greatly affects specific power density, the electrolyte stability voltage window is the primary criterion for electrolyte selection [12,25]. The stability voltage window sets the limits for the voltage that can be applied to the electrodes without causing electrolyte decomposition. This supports the importance of this property since the specific energy density (E) is proportional to the squared voltage. It is also shown in the following equation [2]:

$$E = -\frac{1}{2}CV^2 \quad (4)$$

The ion size of the salts [27] is another important parameter to consider when choosing the electrolyte composition. Regarding the electrolyte solvent, two types of electrolytes have been widely used in supercapacitors, aqueous and organic. A third type of electrolytes are ionic liquids (ILs) (Table 4).

Table 4. Voltage windows and ionic conductivity for aqueous and organic electrolytes and ionic liquids.

Type of Electrolyte	Voltage Window (V)	Ionic Conductivity (mS.cm ⁻¹)
Aqueous	≤1.2 [9,28]	>400 [17,28]
Organic (NEt ₄ BF ₄ /PC)	3.0 [28]	13 [28]
Organic (NEt ₄ BF ₄ /ACN)	2.7 [28]	56 [28]
Ionic Liquids	3–5 [9,17]	<15 [17,28]

The most common aqueous electrolytes are H₂SO₄, KOH, and KCl. They have high ionic conductivity. However, they have a narrow voltage window (approximately 1.2 V) [9]. Low cost, easy handling in an open environment, and the availability of diverse pH values are some of the advantages of using aqueous electrolytes [9,25,63]. The most used organic electrolytes are solvents based either on acetonitrile (ACN) or propylene carbonate (PC). These electrolytes have wider voltage windows (up to about 2.2–3 V) [9] but much lower ionic conductivity than aqueous electrolytes, especially PC, which has more than four times lower ionic conductivity than acetonitrile.

However, acetonitrile is both toxic and flammable, making PC a more attractive option for safety and environmental reasons [9,25,27,28]. Salts liquid (molten) at room-temperature [9,25] are the characteristics of ILs. Furthermore, their stability voltage windows only depend on the electrochemical stability of the ions since they do not contain any solvent. The voltage windows of these electrolytes are wider than both aqueous and

organic electrolytes (approximately up to 3–5 V) [9]. However, they are preferably used at higher temperatures because the ionic conductivity is low at room temperature. The ILs are expected to significantly contribute to improving the performance of supercapacitors, at least for high-temperature operations, as they have many advantages. They have higher energy density and power density than other electrolytes, a well-defined ion size (a solvation shell should not be considered) [16], and are nontoxic, nonflammable, and chemically stable [2,9,25].

(iii) Current collectors:

The transport of the electric current between the electrodes and the external loads is the main role of the current collectors [9,12]. In general, the current collectors provide efficient transfer of electrons to external circuits, which depends on their conductivity. In addition, the charge/discharge process may be accompanied by heat generation at the current collector with low conductivities [64]. Therefore, the current collectors need to have good electrical conductivity in order to reduce the total resistance of the supercapacitor and to increase its specific power [12]. Furthermore, they must resist corrosion, which can be achieved through chemical and electrochemical stability [9,12,17]. Reflecting these factors, stainless steel is the most used in aqueous electrolytes, while aluminum alloys are favored in organic electrolytes, as they have low density and good thermal conductivity [9].

The contact between current collectors and the active layers of the electrodes is another important factor to consider [2,9,12]. It is mentioned that the interface resistance makes a significant contribution to the total resistance, therefore, this kind of contact should be the lowest possible [12]. To achieve this, polymeric binding agents (i.e., Nafion[®] and polytetrafluoroethylene) are employed [9].

(iv) Separators:

The function of the separator is to electrically isolate the two electrodes, which would make it possible to prevent short circuits and guarantee ionic conductivity [12,17]. The separator is generally a porous membrane [12] and several properties need to be considered. The membrane must be electrically non-conductive while electrolytic ions must be permeable with minimum ionic resistance. Moreover, it needs to be chemically resistant (i.e., resistant to electrolytes and electrode materials) [9], thermally resistant [17], flexible (i.e., endure pressure and volume changes), and easily soaked in electrolytes [9]. The cellulose [17] and polymers (e.g., fibrous structure and monolithic network with defined pores) [9] are the materials commonly used.

2. Proposed Strategies for Higher Performance in Supercapacitors: (Nano)Structuring, Electrolyte Composition, Pseudocapacitance, and Hybrid and Composite Electrodes

Research on (i) nanostructuring, (ii) electrolyte composition, (iii) pseudocapacitance behavior, and (iv) hybrid and (v) composite electrodes has been proposed to improve the performance of supercapacitors. These strategies are detailed below.

(i) Nanostructuring

The performance of supercapacitors can be affected by the physical and chemical properties of carbon materials, e.g., pure CNTs. It includes size, purity, shape, defects, annealing, and functionalization. Furthermore, composites such as CNT/oxide and CNT/polymer have shown an increase in capacitance and supercapacitor stability. It has been achieved through optimal engineering of composition, particle size, and coverage [65]. For example, high values of specific capacitance (350 F/g), power density (4.8 kW/kg), and energy density (3.3 kJ/kg) have been shown in pyrrole-treated functionalized SWCNTs [66]. Moreover, 73 wt.% PANI deposited onto SWCNTs have shown high values of specific capacitance (485 F/g), specific power (228 Wh/kg), and specific energy (2250 W/kg) [67].

(ii) Electrolyte Composition

According to the literature, an ideal electrolyte for EDLC must have the following characteristics: a wide electrochemical window (>4), specific conductance of $>75 \text{ mS}\cdot\text{cm}^{-1}$ at room temperature, thermal stability up to $300 \text{ }^\circ\text{C}$, and low toxicity. However, the ionic conductivity is low at room temperature in the case of ionic liquids [25].

Lin, R has studied the influence of the type of electrolyte vs. energy density at different voltage windows. The author confirmed that ionic liquids (ILs) are the most important electrolytes in terms of energy density compared to organic and aqueous electrolytes. ILs operated in a wider voltage window. Li, R also mentioned that the combination of anions and cations influences the composition and associated properties of ILs. Millions of different structures can form an IL. The number of cation and anion combinations can be as high as 10^{18} [58]. However, Aprotic, Protic, and Zwitterionic are the main classes used in different types of applications [68]. Aprotic ILs are most commonly used for EDLC applications as they allow cell voltage to be increased above 3 V. Therefore, ILs are well known for their high electrochemical stability and thermal stability and are largely studied in energy storage devices [69].

(iii) Pseudocapacitance

The pseudocapacitors are another type of technology that provides an increase in the specific capacitance and the energy density. In this technology, charge storage is achieved through a reversible redox reaction within the electrode surface [17,63,70].

Metal oxides, such as RuO_2 [71] and MnO_2 [72], and conducting polymers are the main class of electrode materials used for charge storage in pseudocapacitors [73,74]. However, the redox reactions can affect the cycling stability due to aging.

(iv) Hybrid Electrodes

An ideal storage device that has the high-power density of a supercapacitor and the high energy density of a battery is the primary goal of a hybrid technology. Some examples of asymmetrically structured hybrid supercapacitors have been reported in the literature. The combination of a carbon electrode (of supercapacitor type) with a faradaic electrode (of battery type) is achieved in this kind of technology. However, these hybrid systems have intermediate characteristics. In these systems, the charge/discharge speed is slower than the classic supercapacitor due to the influence of the redox reactions at the faradaic electrode. A shorter lifetime is also caused by the chemical reactions that are due to the consumption of the active material. Considering these characteristics, hybrid supercapacitors have been the subject of numerous studies [22,29,75]. For instance, JSR Micro and JM Energy Corporation proposed two Li-ion hybrid supercapacitors called the 2300 F and 3300 F prototypes. Their energy density is about $10 \text{ Wh}\cdot\text{kg}^{-1}$ [76].

(v) Nanocomposite electrodes

Nanocomposite electrodes have been reported in the literature [77], to improve the performance of supercapacitors. Binary-composite or ternary-composite films have been evaluated, employing various methods of preparation. It has been revealed that high specific capacitances were reached with PANI-CNT [78] or PEDOT-CNT [79,80] composites. It was either enhancing the robustness of the flexible PPy-CNTs [81] or improving the capacitive properties of PTh-CNTs films [82]. Ternary nanocomposites of Mn_3O_4 , TiO_2 , and reduced graphene oxide (RGO) electrodes have been also studied for supercapacitor applications [83]. This material has achieved a specific capacitance of $356 \text{ F}\cdot\text{g}^{-1}$ in 6 M KOH aqueous electrolyte and respectable cycling performance, making it suitable for supercapacitors. In addition, a summary of these kinds of materials including specific capacitance and type of electrolyte is presented in Table 5.

Table 5. Summary of various metal oxide/carbon composite electrodes for supercapacitors [84], open access.

Material	Potential Window/V	Specific Capacitance /F g ⁻¹ (Scan Rate or Current Density)	Electrolyte	Retention/% (Cycles)
ZrO ₂ carbon nanofibers	0–1	140 (1 A g ⁻¹)	6 M KOH	82.6 (10,000)
RuNi ₂ O ₄ /rGO composites	0–1	792 (1 A g ⁻¹)	0.5 M Na ₂ SO ₄	93 (10,000)
NiO/activated carbon composites	0–0.4	568.7 (0.5 A g ⁻¹)	2 M KOH	90.6 (5000)
Ni _{0.25} Co _{0.25} oxide/carbon nanofibers	–1–0	431.2 (1 A g ⁻¹)	6 M KOH	94 (2000)
MnO/Fe ₂ O ₃ /carbon nanofibers	0–1	437 (1 A g ⁻¹)	6 M KOH	94 (10,000)
ZnO/MnO/carbon nanofibers	0–1.6	1080 (1 A g ⁻¹)	6 M KOH	96 (800)
Au-Mn ₃ O ₄ /GO nanocomposites	–0.2–1	475 (1 A g ⁻¹)	0.5 M H ₂ SO ₄	94 (10,000)
Bi ₂ O ₃ /MWCNT composites	–1.2–0.2	437 (1 A g ⁻¹)	6 M KOH	88.7 (3000)
NiO/MnO ₂ /MWCNT composites	0–0.55	1320 (1 A g ⁻¹)	2 M KOH	93.5 (3000)
Carbon nanosheets/MnO ₂ /NiCo ₂ O ₄ composites	0–1	1254 (1 A g ⁻¹)	1 M KOH	81.9 (5000)
ZrO ₂ /C nanocomposites NiO/porous amorphous carbon nanostructure	0–1	214 (1.5 A g ⁻¹)	1 M H ₂ SO ₄	97 (2000)
NiO/porous amorphous carbon nanostructure	0–1.6	508 (1 A g ⁻¹)	6 M KOH	78 (3000)
Defective mesoporous carbon/MnO ₂ nanocomposites	–0.8–0.8	292 (0.5 A g ⁻¹)	1 M Na ₂ SO ₄	79 (2000)

In an overview, the specific capacitance of the representative EDLCs and pseudocapacitors systems based on various active materials are shown in Figure 4.

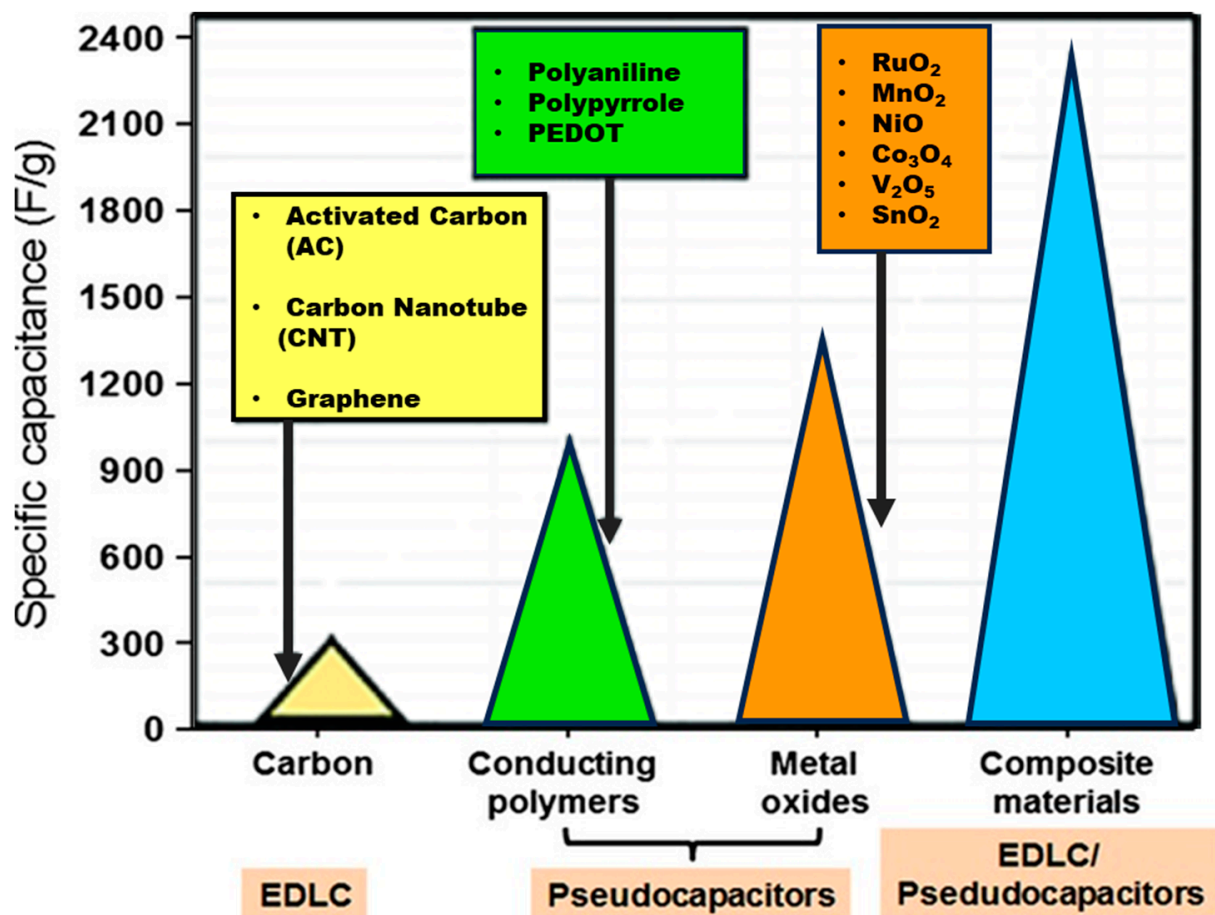


Figure 4. Comparison of various materials (electrodes) according to their specific capacitance for different supercapacitor applications. Adapted from Ref. [85] with permission from Elsevier (copyright 2020) and Ref. [86] open access.

Furthermore, Table 6 shows a comparison between the different types of supercapacitors. Some advantages and disadvantages are also included.

Table 6. Comparison between EDLCs, pseudocapacitors, and hybrid capacitors. Modified from Ref. [87] open access.

Parameters	EDLC	Pseudocapacitor	Hybrid Capacitor
Material	Carbon-based materials, e.g., activated carbon, carbon nanotubes	Metal oxides, conducting polymers, e.g., NiO, MgO, PANI	Metal oxide/carbon-based materials, conducting polymer/carbon-based materials, e.g., Ni(OH) ₂ /rGO, PANI/rGO
Storage mechanism	Non-faradic/electrostatic, electrical charge stored at the metal/electrolyte interface	Faradic, reversible redox reaction	Both faradic and non-faradic
Specific capacitance	Lower	Higher	Higher
Energy density	Low	High	High
Cycle Life/stability	High	Low	High
Voltage operation	High voltage and high-power operation	Low-voltage functioning is restricted by electrochemistry and the solvent's solvent decomposition voltage	Increased cell voltage
Charge/discharge speed	Faster	---	Slower

3. Diagnostic Tools for Electrode Materials in Energy Storage

To improve the performances of supercapacitors, it is necessary to use appropriate tools to examine the electrochemical behavior of the different electrode materials. Electrochemical techniques such as (i) cyclic voltammetry, (ii) galvanostatic charge-discharge and (iii) electrochemical impedance spectroscopy, (iv) electrochemical quartz crystal microbalance (EQCM), (v) *ac*-electrogravimetry, (vi) NMR spectroscopy, and (vii) computer simulation will be discussed in this section.

(i) Cyclic Voltammetry (CV)

Cyclic voltammetry is a potentiodynamic electrochemical measurement technique. It measures current as a function of potential. For that, two successive potential scans (cyclic) are imposed between the working electrode and the reference electrode. In this way, the current is measured across the working electrode and the counter electrode [88,89]. This information is plotted as current (*i*/A) in the function of applied potential (*E*/V) to provide the cyclic voltammogram trace. Furthermore, the potential range can be limited by the electrolyte stability window.

It has been reported in the literature, that cyclic voltammetry provides quantitative and qualitative information on the capacitive behavior at the electrode/electrolyte interface. This technique also identifies the presence of parasitic faradic reactions [17]. A typical cyclic voltammogram curve, for capacitance diagnosis, is shown in Figure 5.

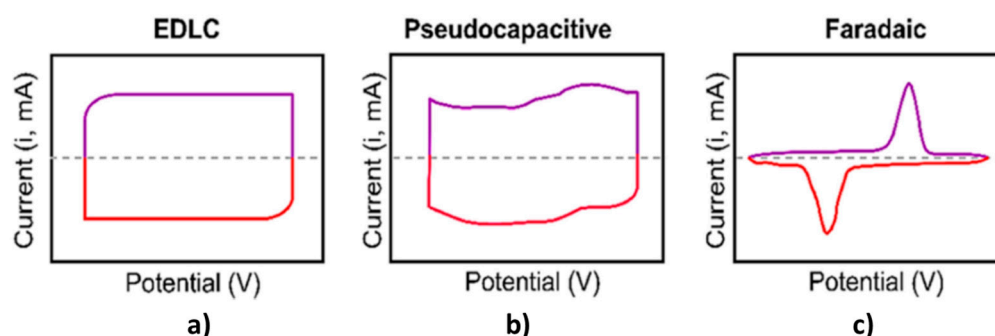


Figure 5. Cyclic voltammogram curves of (a) ideal EDLC, (b) pseudocapacitor (c) and faradaic type materials. Adapted from Ref. [90], open access. Pink color corresponds to oxidation domain and red color corresponds to reduction domain.

In Figure 5a, the rectangular CV represents an ideal supercapacitor response. However, in practice, an almost deformed rectangular shape can be obtained due to redox reactions, characteristic of pseudocapacitive behavior (Figure 5b). Finally, two redox peaks are observed in Figure 5c, which is predominantly faradaic behavior.

CV plots from 3E (three electrodes) and symmetric 2E (two electrodes) systems have also been studied by Verma et al. [91]. The CV results of different samples related to high specific capacitance values were attributed more to 3E systems than to 2E systems (e.g., GO/PANI/CuFe₂O₄ ternary gave the highest specific capacitance value of 790.12 F/g and 357.28 F/g at 1 mV/s and 1 A/g from 3E and symmetric 2E device systems, respectively).

(ii) Galvanostatic Charge-Discharge method (GCD)

The capacitance, resistance, and cyclability of the electrode materials are measured by GCD. This technique consists of carrying out charge/discharge cycles. The potential response is measured over time when a constant current density is applied [92] (Figure 6). Through the slope of the discharge curve shown in Figure 6, the cell capacitance (C) can be calculated using the following equation [93]:

$$C = \frac{I}{\frac{dV}{dt}} \tag{5}$$

where *I* is the discharge current and *dV/dt* is the slope of the discharge curve. The specific capacitance *C_s* is related to the capacitance of the cell *C* by:

$$C_s = \frac{2C}{m} \tag{6}$$

where *m* is the mass per electrode of the active material.

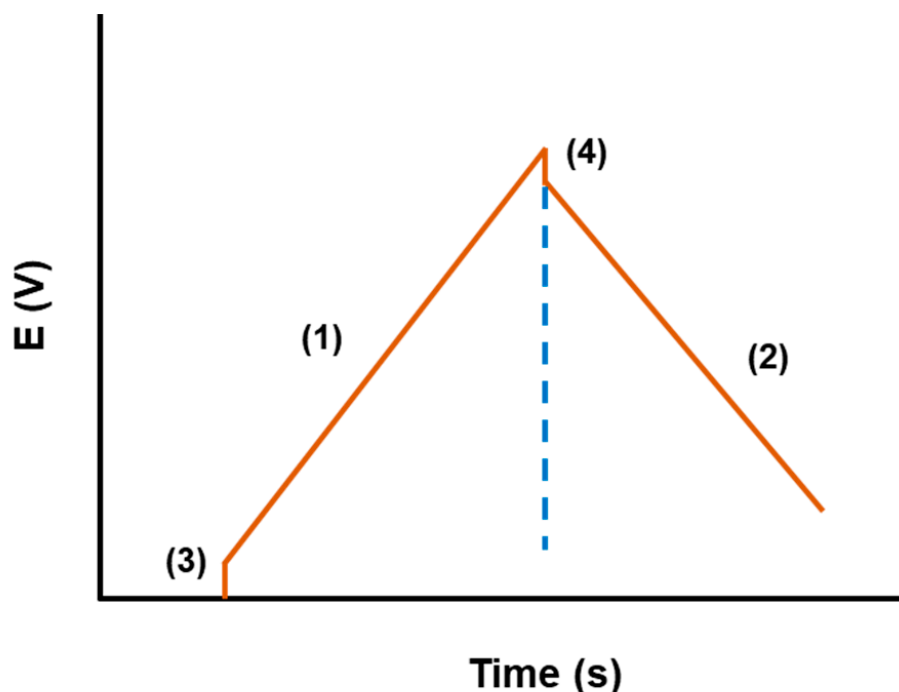


Figure 6. Typical curve of a galvanostatic charge-discharge process. (1) The cell behavior during charging; (2) the cell behavior during discharge; (3) the initial process; (4) this segment is responsible for the negative resistive ohmic loss associated with the resistance of the cell.

(iii) Electrochemical Impedance Spectroscopy (EIS)

The EIS measurements are based on frequency modulation. This technique provides qualitative information about the studied system (capacitive, resistive, diffusive behavior, etc.) and allows the calculation of the capacitance of the electrodes [92]. Electrochemical impedance is based on the collection of an alternating current (AC) resulting from applying a sinusoidal potential perturbation with a small amplitude (typically 10 mV rms) [94]. The Nyquist diagram ($-ImZ$, ReZ Cartesian coordinates) and the Bode diagram (polar coordinates) are the plots normally used for EIS measurements.

In the literature, there are several works employing EIS to study carbon electrodes in supercapacitors [30,95]. Rajasekaran et al. [96] performed studies of impedance on activated carbon (AC) materials. This material was also tested in different electrolytes such as KOH, Na_2SO_4 , and H_2SO_4 .

Figure 7 shows the Nyquist plots of RCS-AC electrodes from EIS measurements in the frequency range of 100 kHz to 10 MHz. Here, three different frequency regions are observed in the electrochemical process. At the low-frequency region, a quasi-vertical line is observed in all electrolytes, which is indicative of capacitive behavior. In the zoomed region (inset of Figure 7), a semicircle is observed due to the presence of resistance in the electrode. It is known that a Warburg region is a transition range between the low-frequency and high-frequency ranges. In this way, the authors concluded that the width of the impedance arc at this transition area indicates resistance due to ion diffusion and transportation at the electrode/electrolytes interface.

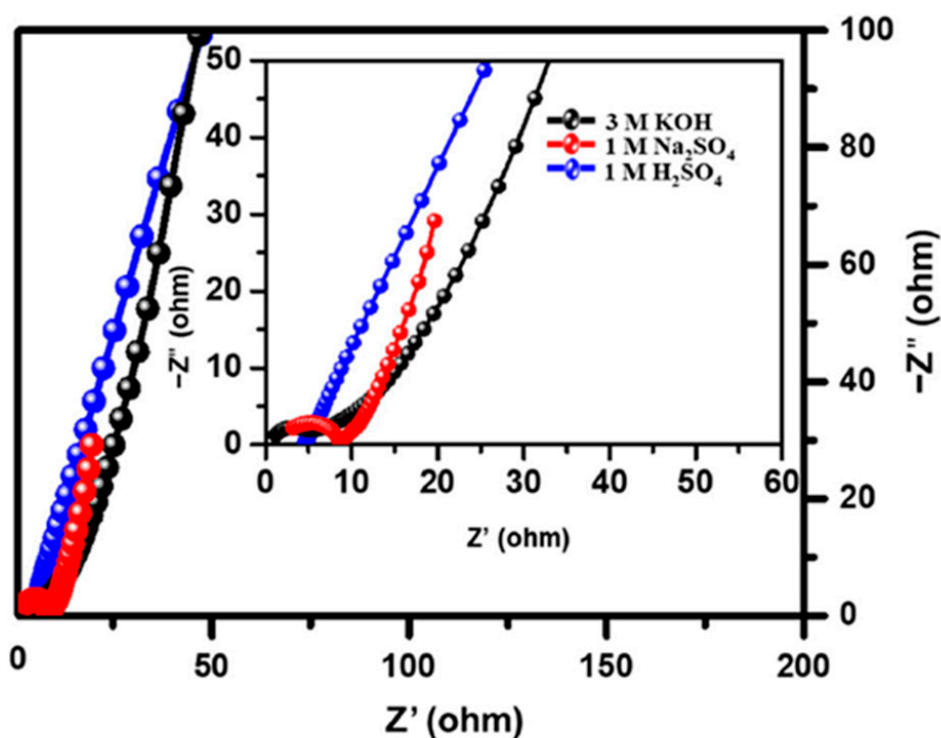


Figure 7. Nyquist plots of the activated carbon electrode in different electrolytes (Inset—An expanded representation of the EIS plot in the high-frequency region). Adapted from Ref. [96], open access.

Escobar-Teran et al. [97] also investigated the capacitive behavior of SWCNT electrodes using electrochemical impedance. The carbon electrodes were tested in a NaCl aqueous electrolyte and at different electrolyte pH conditions. Figure 8 shows the electrochemical impedance responses of the SWCNT at pH 2, pH 7, and pH 10.

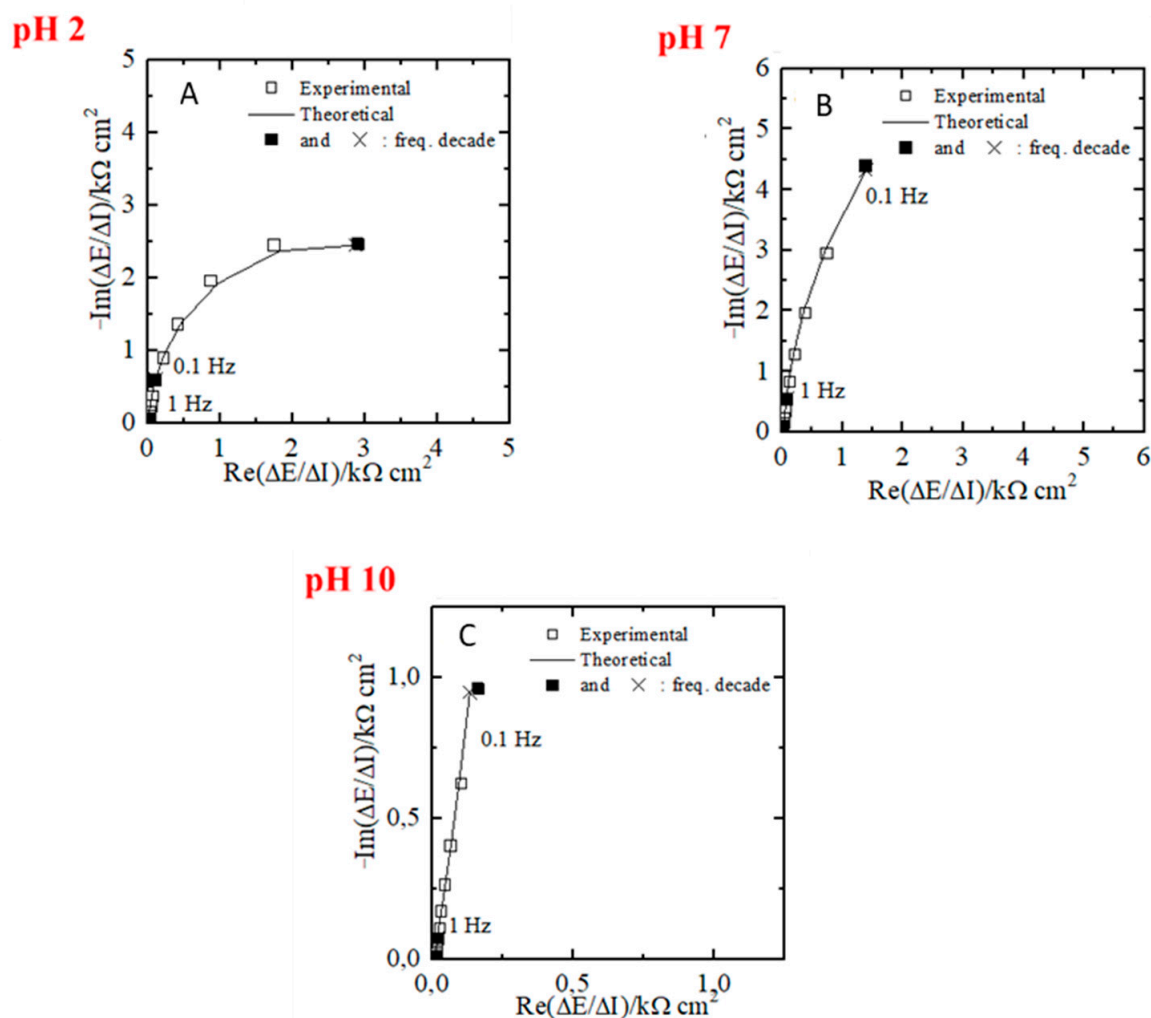


Figure 8. Experimental and theoretical electrochemical impedance data of the SWCNT thin film in 0.5 M NaCl measured at -0.4 V vs. Ag/AgCl and at pH 2, pH 7, and pH 10, respectively (A–C) $\frac{\Delta E}{\Delta I}(\omega)$. Reproduced from Ref. [97] with permission from the American Chemical Society (copyright 2019).

They are presented in a comparative way at a selected potential (-0.4 V). The electrochemical impedance responses, $\frac{\Delta E}{\Delta I}(\omega)$ show a distorted straight line, which is due to a multi-ion transfer contribution for the three pH values (Figure 8A–C). Particularly, at pH 2 (Figure 8A), the distortion is more significant than at pH 7 and pH 10 (Figure 8B,C). The authors concluded that it is probably due to the amplified effect of H^+ reduction by the high proton concentration for the pH 2 case.

(iv) Electrochemical Quartz Crystal Microbalance (EQCM)

EQCM is a coupled method between Quartz Crystal Microbalance (QCM) with an electrochemical measurement technique [98,99]. As it is often coupled with cyclic voltammetry, cyclic electrogravimetry is another name for this technique [100].

During an electrochemical process, gravimetric EQCM is capable of quantitatively measuring small mass changes occurring at the electrode surface. It can detect mass changes in the order of 1 nanogram [101]. Various approaches have been investigated through this technique, for example, metal electrodeposition [102–104], electrocrystallization [105], electrochromic reactions [106], intercalation [107], and as well as adsorption and mass variations associated with electrolyte-ion movement [108–110]. Furthermore, the viscoelastic properties can be studied through the EQCM with dissipation monitoring (EQCM-D), e.g., formation of a solid electrolyte interface (SEI) layer as well as the complex mass changes in the electrodes [111–114]. Identification of the effect of various parameters such as the

nature of the electrolytes/ions or the binder on the change in the structure of the electrodes is possible through this acoustic technique [115].

It has been shown that the EQCM technique provides information on the capacitive behavior of carbon electrodes by analyzing the capacitive current and the resulting mass changes in the carbon film electrodes. Examining the literature, a certain number of papers employing EQCM to study carbon materials have been found [116,117]. Maier et al. [118] investigated, in carbon micropores, the effect of specific adsorption of cations and their size on the charge compensation mechanism. This material was investigated using EQCM technique and tested in 0.5 M NH_4Cl . This technique revealed a complicated interplay between the adsorption of NH_4^+ cations and the desorption of Cl^- anions inside carbon micropores at low surface charge densities, which results in failure of their permselectivity. The complete exclusion (desorption) of Cl^- co ions is due to the higher negative densities, imparting purely permselective behavior in carbon micropores (Figure 9).

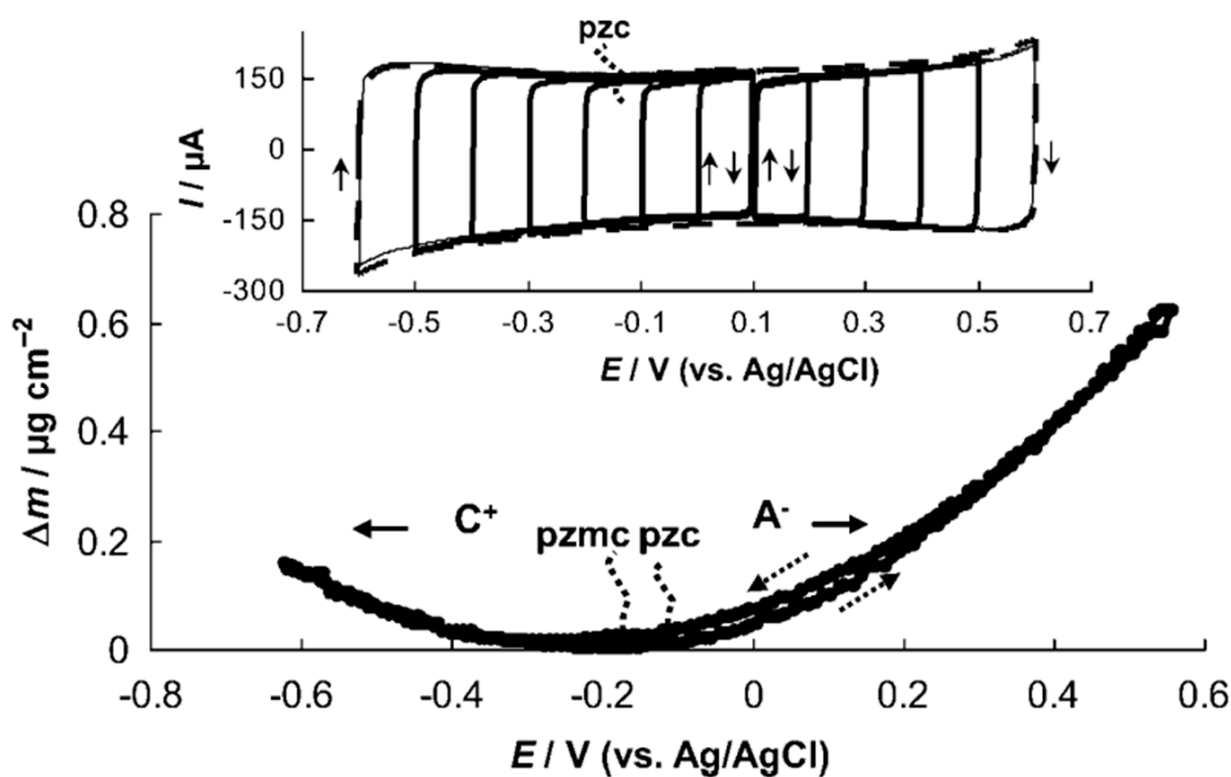


Figure 9. Mass change in the carbon electrode in a 0.5 M aqueous solution of NH_4Cl (scan rate = 20 mVs^{-1}) measured simultaneously with the CV of the largest 1.2 V amplitude (see inset, broken line). The inset also shows a series of CVs measured with different potential amplitudes. Reproduced from Ref. [118] with permission from John Wiley & Sons (copyright 2011).

The authors introduced two terms in the context of these measurements: the potential of zero charge (PZC) and the potential of zero mass change (PZMC) to quantitatively correlate the mass changes in the adsorbed ions and solvent molecules with the potential-induced variation of the electrode charge density. According to a conventional point of view, the adsorption of anions and cations into carbon micropores occurs at $Q > 0$ and $Q < 0$, respectively. In this way, the PZMC should coincide with the PZC. However, the PZMC obtained from the EQCM does not coincide with the PZC of the electrode according to Figure 9. It is because the former may depend on the dynamics of formation of the ionic part of the electric double layer (EDL), that is, on the relation between the fluxes of counterions (anions at $Q > 0$ and cations at $Q < 0$) and co-ions (cations at $Q > 0$ and anions at $Q < 0$).

Escobar-Teran et al. [119] investigated the capacitive behavior of SWCNT-based thin films via EQCM in 0.5 M aqueous NaCl. A quasi-rectangular cyclic voltammetry (CV) response is shown in Figure 10A, which indicates that the charge storage is mainly due to the reversible electroadsorption of the ions. Figure 10B shows the corresponding mass variations followed by simultaneous QCM measurements as a function of potential. According to authors, a change in slope around 0.1 V vs. Ag/AgCl where $\frac{\Delta m}{\Delta E} < 0$ and $\frac{\Delta m}{\Delta E} > 0$ for the transfer of cations and the anions is observed in Figure 10B, which indicates that the point of zero charge (PZC) is around this value.

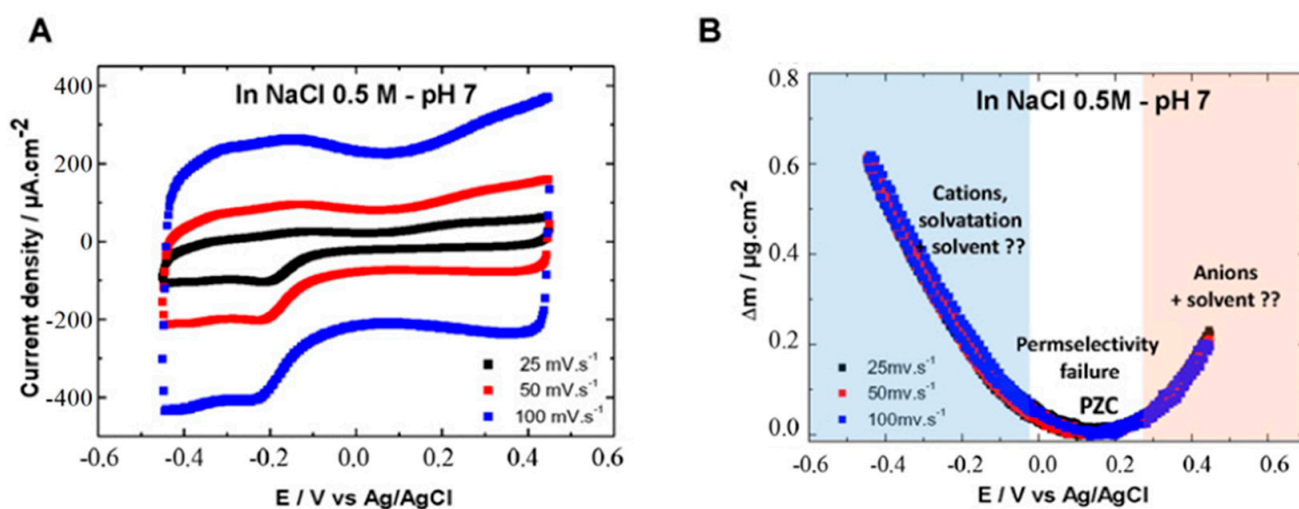


Figure 10. The CV curves (A) and the simultaneous mass responses (B) of the SWCNT-based thin films in 0.5 M NaCl at pH = 7. Reproduced from Ref. [119] with permission from Elsevier (copyright 2016).

Another study [97] has investigated the influence of electrolyte pH on CNTs through the EQCM technique. Figure 11 shows the EQCM results of SWCNT film electrodes obtained in aqueous electrolytes of 0.5 M NaCl at pH 2, pH 7, and pH 10. It is noticed the capacitive current increases when the scan rate increases (Figure 11A–C). In this study, the SWCNT film electrodes show quasi-rectangular shaped responses, meaning that the charge storage is due to the reversible electroadsorption of electrolyte ions. A slight faradaic contribution is observed, which is probably due to the remaining surface functionalities on the nanotubes. A pH dependency on the mass changes in the SWCNT electrodes is observed. It shows a change in slope ($\frac{\Delta m}{\Delta E} < 0$ for the transfer of cations and $\frac{\Delta m}{\Delta E} > 0$ for anions), around -0.1 V, 0.1 V, and ~ 0.125 V vs. Ag/AgCl, at pH = 2, 7, and 10, respectively. It means that the points of zero charge (PZC) correspond to these values (Figure 11A–C). In other words, the PZC depends on the pH range, and it is significantly different at pH = 2 compared to pH = 7 and pH = 10.

The capacitive charge storage behavior of the ERGO (Electrochemical Reduced Graphene Oxide) thin film electrodes was also studied by Gouba et al. [50] using the EQCM technique. The carbon electrodes were tested in different aqueous electrolytes such as LiCl, NaCl, and KCl (Figure 12). Figure 12A shows the CV responses of ERGO electrodes obtained in the three aqueous electrolytes at 100 mV s^{-1} . In this study, the ERGO electrodes show quasi-rectangular CV responses indicating that the charge storage is mainly due to the reversible electroadsorption of the electrolyte ions. According to the authors, the slight distortion observed in CV responses is due to the presence of a slight faradaic contribution to the charge storage.

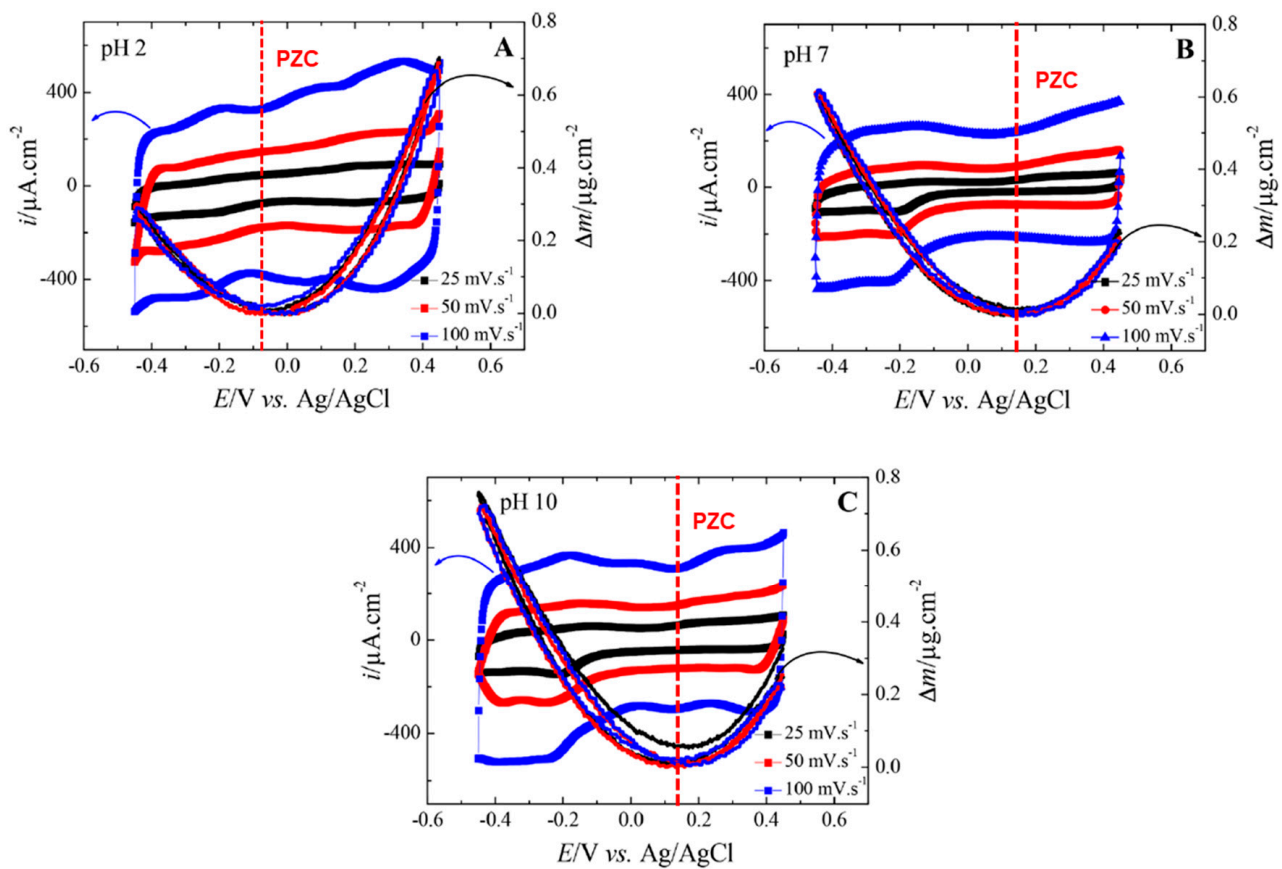


Figure 11. EQCM responses of SWCNT thin film measured in 0.5 M NaCl at pH 2 (A), pH 7 (B), and pH 10 (C). Reproduced from Ref. [97] with permission from the American Chemical Society (Copyright 2019).

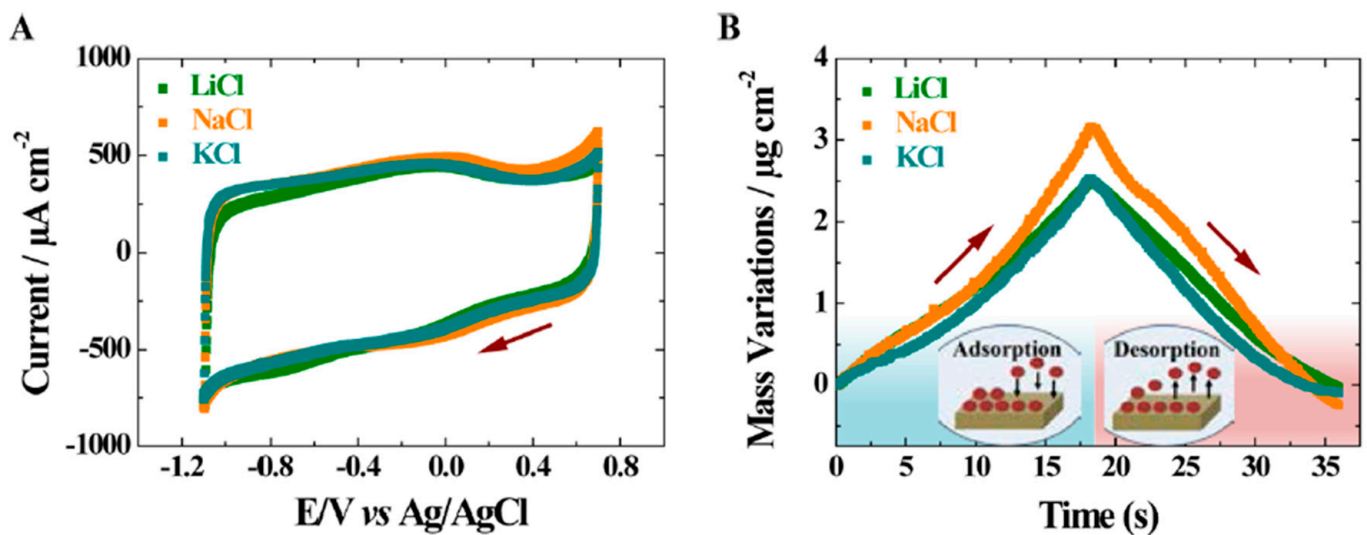


Figure 12. CV curves (A) and simultaneously obtained mass responses (B) of ERGO thin films measured in 0.5 M aqueous solution of LiCl, NaCl, and KCl at 100 mV s⁻¹. The arrows correspond to the scan direction of the potential in (A). CV scan starts from the anodic potentials towards cathodic potentials. Reproduced from Ref. [50] with permission from the American Chemical Society (copyright 2017).

Figure 12B shows the mass changes in the ERGO electrodes. It is observed in Figure 12B that the mass variations are almost identical when measured in aqueous LiCl and KCl solutions and simultaneously similar current values are obtained in the same solutions. According to the authors is due that the same amount of charge is electroadsorbed at the electrode/electrolyte interface. However, it would not be consistent considering the molecular weight of the ions and if only the cationic species contribute to the electroadsorption process. The authors explain that the Li^+ species are electroadsorbed together with free solvent molecules, and this phenomenon is more pronounced compared to that which occurs in aqueous KCl electrolytes. Furthermore, both species (Li^+ and K^+) are electroadsorbed in their hydrated form but they differ in the degrees of hydration.

The capacitive behavior in nanocomposite carbon film electrodes was also investigated by Escobar-Teran et al. [5]. The EQCM technique was used to investigate the electrochemical behavior of SWCNT/PPy composite electrodes in aqueous electrolyte NaCl 0.5 M (Figure 13). The authors observed a slight contribution of the PPy component to the CV responses (Figure 13a), as compared to that of pristine SWCNTs [119]. In contrast, a significant difference in terms of amplitude and shape is observed in the mass response of carbon film compared to SWCNT alone (Figure 13b). According to the authors, these qualitative observations show that the presence of PPy changes the interfacial ion exchange behavior of SWCNTs.

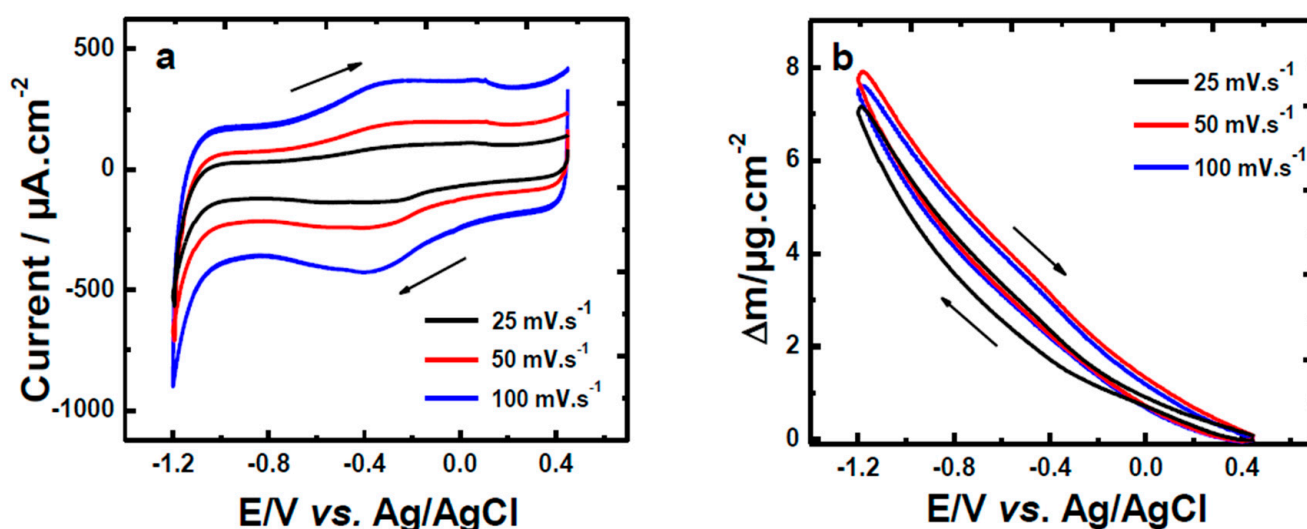


Figure 13. EQCM results of SWCNT/PPy composite thin films: (a) current vs. potential; (b) mass variation vs. potential measured in aqueous electrolyte 0.5 M NaCl. The arrows correspond to the scan direction of the potential in (A). CV scan starts from the anodic potentials towards cathodic potentials [5], open access.

(v) *ac*-electrogravimetry

Since its development in 1986, *ac*-electrogravimetry has been shown to be a very promising tool for unraveling the role of each species involved at the electrode/electrolyte interface. This laboratory-developed technique combines fast quartz crystal microbalance (QCM) with electrochemical impedance spectroscopy (EIS). In addition, this technique provides relevant information such as (i) identification of species involved (with their flux directions) at the electrode/electrolyte interface, (ii) separation of charged and non-charged species, (iii) determination of their kinetics, and (iv) variation of their relative concentrations [120–122]. Escobar-Teran et al. [4] used *ac*-electrogravimetry to study the electrochemical behavior of carbon nanotubes in aqueous electrolytes. In this work, the charge/potential and electrogravimetric transfer functions were established considering all ionic species involved. Then, the transfer functions were used to fit the experimental results using kinetic parameters: K_i (kinetics of ionic transfer) and G_i (inverse of transfer

resistance), respectively, considering the transfer of ions and solvent molecules at the electrode/electrolyte interface. Figure 14A,B show the experimental transfer functions $\frac{\Delta q}{\Delta E}(\omega)$ and $\frac{\Delta m}{\Delta E}(\omega)$ fitted by theoretical equations explained in previous papers [4,5,119]. With the frequency variation, as shown in Figure 14B, different ionic species can be discriminated. From Figure 14C, the result shows that the hydrated Na^+ ion mass transfer is faster than that of protons (H^+).

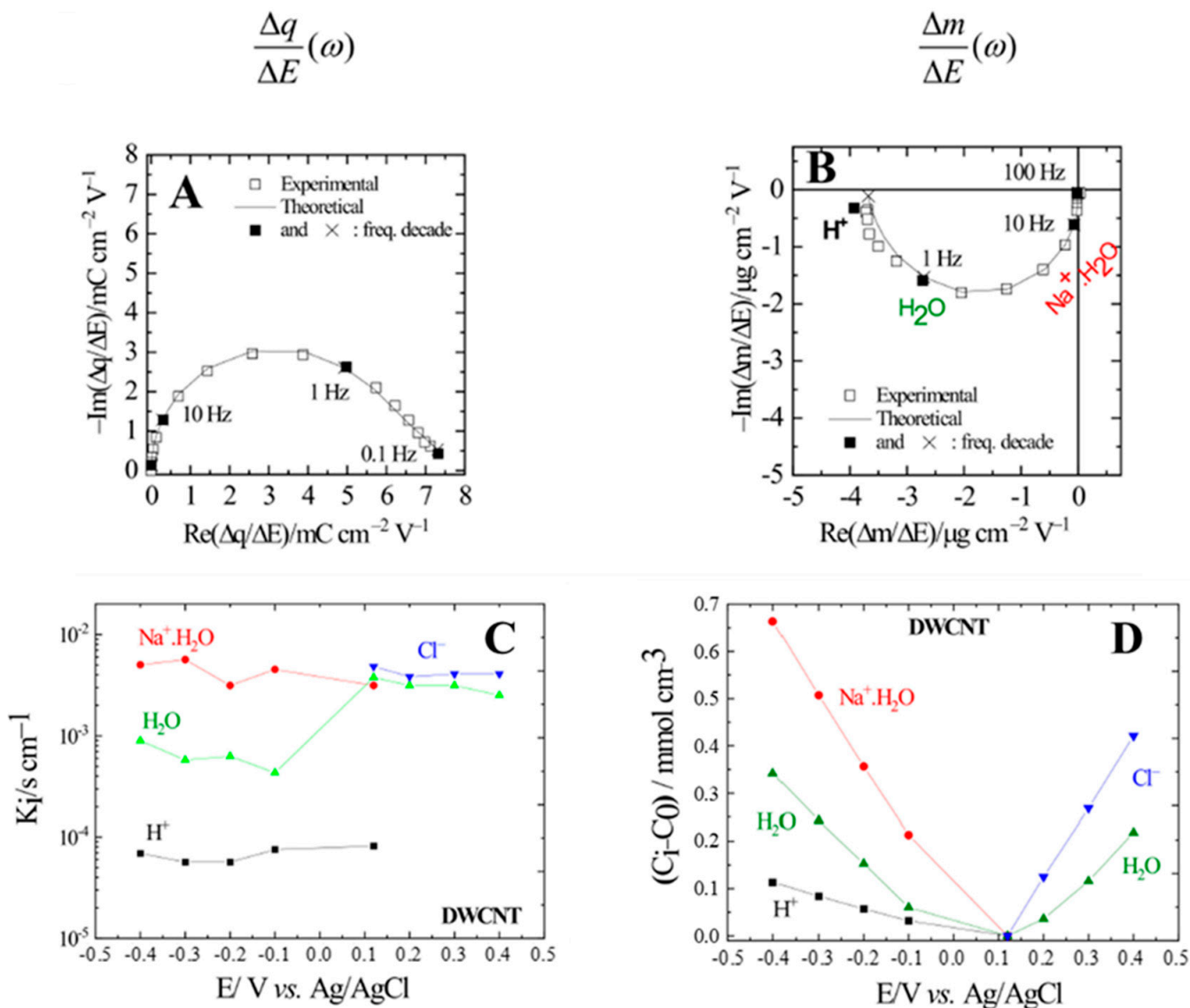


Figure 14. Experimental and theoretical AC-electrogravimetric data of the CNT thin films in 0.5 M NaCl measured at 0.4 V vs. Ag/AgCl. (A) $\frac{\Delta q}{\Delta E}(\omega)$, (B) $\frac{\Delta m}{\Delta E}(\omega)$, (C) K_i , and (D) C_i-C_0 [4], open access.

In addition, the free water molecules follow the transfer of the hydrated Na^+ and Cl^- , which is due to an electrodragging phenomenon. Finally, the relative concentration changes in each species estimated by ac-electrogravimetry allow us to distinguish between the contributions of the different ionic species (Figure 14D).

In summary, the ionic fluxes in carbon nanotubes during the charge/discharge can be analyzed in detail using the ac-electrogravimetry technique.

(vi) Nuclear magnetic resonance spectroscopy (NMR)

NMR spectroscopy is one of the promising techniques used to study the ion environments in supercapacitor electrodes and quantify changes in the populations of adsorbed

species during charging [123–130]. The working principle of the NMR regarding the confinement of ions in nanopores is based on the resonance shift of the target electrolyte ions to a lower frequency due to the distribution of delocalized electrons present on the carbon surface that shields the signal [3].

The NMR spectra of supercapacitor electrodes offer a considerable amount of relevant information (i) the number of in-pore anions and cations can be determined through the intensities of the in-pore resonances and thus the composition of carbon pores and the charging mechanisms of supercapacitors can be studied, (ii) the chemical shift difference between the in-pore and ex-pore resonances provide information about the structure of the carbon, and (iii) the line width of the in-pore resonance can provide information about the dynamics of the ions in the pore [123].

Forse et al. [129] studied the ion dynamics and charge storage in ionic liquid supercapacitors through NMR. The authors found that the adsorption and desorption of anions plays a more dominant role than that of the cations in the charge mechanism. Later, Forse et al. [124] investigated the ion dynamics in supercapacitor electrodes using in situ diffusion NMR spectroscopy. The authors found that the concentration of electrolyte and carbon pore size distributions affect in-pore diffusion and the movement of ions in and out of the nanopores. These findings are very significant to fully unravel the relationships between material properties and performance in supercapacitors.

(vii) Computer Simulations

The simulation of electrochemical systems has become an important topic for understanding the molecular mechanisms involved in energy storage devices [131,132]. Such simulations concern bulk electrode materials and electrolytes whose properties need to be well characterized and rationalized, but more and more effort is being devoted to the description of charge storage mechanisms [131].

The theories of Gouy–Chapman–Stern based on the Poisson–Boltzmann method have been used to explain the charge storage mechanisms (See Figure 15). However, this method is not suited for supercapacitors since field theories become inadequate when the electrostatic correlations between ions and excluded volume effects can no longer be neglected [133,134].

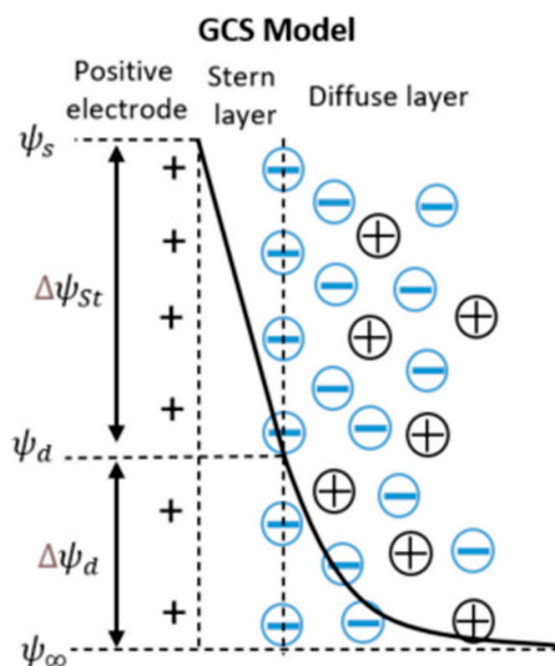


Figure 15. Schematic view of Gouy–Chapman–Stern (GCS). Adapted from Ref. [135], open access.

Computational modeling methods such as molecular dynamics (MD) [136,137] and Monte Carlo (MC) simulations [138], and density functional theory (DFT) [139], are being used for exploring charge storage mechanisms in energy storage devices. Such theoretical methods are principally useful for gaining insight into charging mechanisms when combined with in situ experimental techniques [140].

Molecular dynamics (MD) has been used to explain the ion desolvation process in nanopores when operating in aqueous electrolytes [141–143]. Furthermore, Huang et al. [142] simulated a series of organic electrolytes. The authors demonstrated that the optimal capacitance is obtained when the ratio between the size of the nanopore and the size of the ion is close. Merlet et al. [144] used MD simulation to calculate the degree of confinement of the adsorbed ions and characterize different sites with various morphology of carbide CDC materials. The DFT method is generally used in gas sorption experiments. Particularly, it is used to estimate the pore size distribution and accessible surface area [139]. Monte Carlo simulation and in situ small-angle X-ray scattering (SAXS) have been used to investigate the degree of confinement (DoC) of ions in micropores for an aqueous electrolyte [145].

4. Advantages and Challenges of Main Techniques Used in Energy Storage

The main techniques, commonly used to explain the charge storage mechanisms in electrode materials and covered in this review, include NMR spectroscopy, EQCM, as well as non-classical EQCM based method, i.e., *ac*-electrogravimetry. Computer Simulations have also been shown to provide a significant understanding of the charge storage phenomena. Advantages and challenges are detailed in Figure 16.

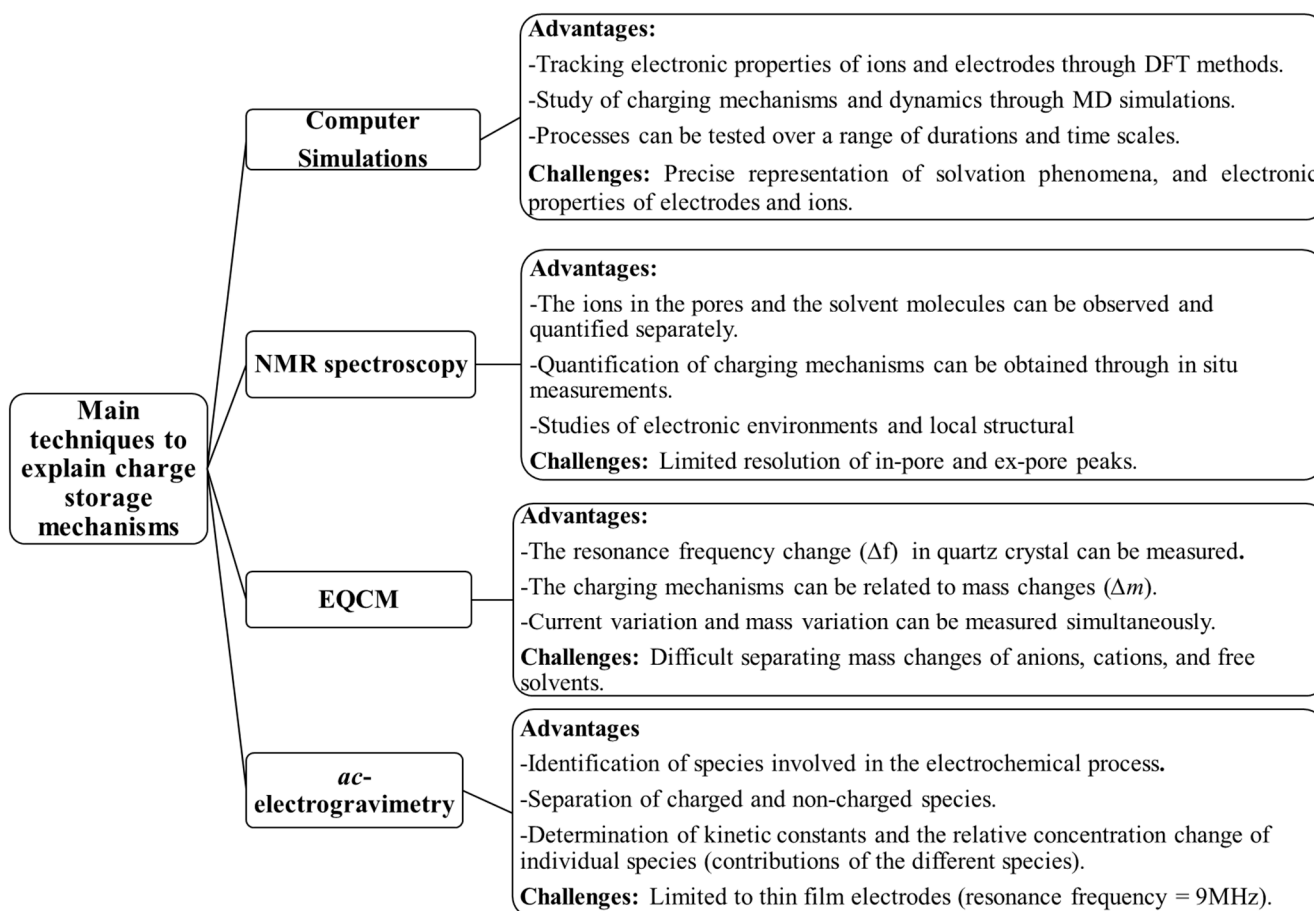


Figure 16. Advantages and challenges of main techniques to explain charge storage mechanisms.

5. Summary and Perspectives

Carbon electrode materials have been extensively studied for electrochemical double-layer capacitors (EDLC). The relationship between the pore size and the ion size is an important factor to consider in order to maximize the specific capacity [119]. The questions related to charging mechanisms are experimentally difficult since there are no appropriate electrochemical or physicochemical techniques that allow direct access to such information. The electrochemical quartz crystal microbalance (EQCM) technique has begun to address these questions. The EQCM technique was also combined with electronic conductance studies or with nuclear magnetic resonance (NMR) to access a complete description of the electrical double layer [109,127]. Furthermore, in situ SAS techniques and other techniques, such as in situ XRD, in situ infrared spectroelectrochemical, etc., have been found to be useful for investigating ion adsorption on nanoporous carbon [3].

However, the dynamic aspects of ion electroadsorption within carbon electrode materials remain a partially unresolved problem with these techniques. Consequently, some research groups have used coupled methods/techniques to better understand the charge storage mechanisms. For instance, the *ac*-electrogravimetry (coupling between fast QCM and EIS) technique has been largely used to study the capacitive behavior in carbon materials since this technique provides relevant information concerning the identification and separation of charged and non-charged species, the determination of kinetic constants and relative concentration/contribution of individual species [4,5,50,97,119]. In situ or operando techniques with simulation or modeling are another powerful tool for extracting additional information, such as the distribution and population of ions on carbon nanopores [3]. Reviewing the literature, we consider that the coupling between two methods/techniques provides a better understanding of the charge storage mechanisms in energy storage devices.

The choice of type of material and electrolyte-ion to improve the performance of the supercapacitor electrodes has been widely studied in the literature. However, the choice of a characterization technique that allows us a deeper understanding of the interfacial charge storage mechanisms is also crucial in the elaboration and performance of the electrode material.

In this way, this review focused mainly on the study of charge storage mechanisms using electrochemical techniques as opposed to the strategies that improve the performance of supercapacitors.

Author Contributions: F.E.-T. designed, wrote, and selected the content and drafted the manuscript. H.P. and O.S. supervised and completed the manuscript. All authors have read and agreed to the published version of the manuscript.

Funding: F.E.-T. thanks the (Secretariat of Higher Education, Science, Technology and Innovation (SENESCYT)-Ecuador for the financial support during his Ph.D. thesis. Agreement No. SENESCYT-DMPF-20212-1476-MI of 19 November 2012.

Data Availability Statement: Not applicable.

Conflicts of Interest: The authors declare no conflict of interest.

References

1. Kabeyi, M.J.B.; Olanrewaju, O.A. Sustainable Energy Transition for Renewable and Low Carbon Grid Electricity Generation and Supply. *Front. Energy Res.* **2022**, *9*, 1032. [[CrossRef](#)]
2. Simon, P.; Gogotsi, Y. Materials for electrochemical capacitors. *Nat Mater* **2008**, *7*, 845–854. [[CrossRef](#)] [[PubMed](#)]
3. Shao, H.; Wu, Y.-C.; Lin, Z.; Taberna, P.-L.; Simon, P. Nanoporous carbon for electrochemical capacitive energy storage. *Chem. Soc. Rev.* **2020**, *49*, 3005–3039. [[CrossRef](#)]
4. Escobar-Teran, F.; Perrot, H.; Sel, O. Ion Dynamics at the Carbon Electrode/Electrolyte Interface: Influence of Carbon Nanotubes Types. *Materials* **2022**, *15*, 1867. [[CrossRef](#)]
5. Escobar-Teran, F.; Perrot, H.; Sel, O. Single Wall Carbon Nanotubes/Polypyrrole Composite Thin Film Electrodes: Investigation of Interfacial Ion Exchange Behavior. *J. Compos. Sci.* **2021**, *5*, 25. [[CrossRef](#)]

6. Banerjee, S.; De, B.; Sinha, P.; Cherusseri, J.; Kar, K.K. Applications of Supercapacitors. In *Handbook of Nanocomposite Supercapacitor Materials I: Characteristics*; Kar, K.K., Ed.; Springer International Publishing: Cham, Switzerland, 2020; pp. 341–350. [[CrossRef](#)]
7. Devi, S.B.; Vignesh, V.; Kumar, P.V.; Oh, M.S.; Navamathavan, R. Chapter 19—Transport supercapacitors. In *Smart Supercapacitors*; Hussain, C.M., Ahamed, M.B., Eds.; Elsevier: Amsterdam, The Netherlands, 2023; pp. 503–534. [[CrossRef](#)]
8. Evanko, B.; Boettcher, S.W.; Yoo, S.J.; Stucky, G.D. Redox-Enhanced Electrochemical Capacitors: Status, Opportunity, and Best Practices for Performance Evaluation. *ACS Energy Lett.* **2017**, *2*, 2581–2590. [[CrossRef](#)]
9. Kim, B.K.; Sy, S.; Yu, A.; Zhang, J. Electrochemical Supercapacitors for Energy Storage and Conversion. In *Handbook of Clean Energy Systems*; John Wiley & Sons, Ltd.: Hoboken, NJ, USA, 2015. [[CrossRef](#)]
10. Zhai, Z.; Zhang, L.; Du, T.; Ren, B.; Xu, Y.; Wang, S.; Miao, J.; Liu, Z. A review of carbon materials for supercapacitors. *Mater. Des.* **2022**, *221*, 111017. [[CrossRef](#)]
11. Lin, R. Formulation of Electrolytes Based on Ionic Liquids for Supercapacitor Applications. Ph. D. Thesis, Sciences de la Matière, Université de Toulouse, Toulouse, France, 2012.
12. Benhaddad, L. Elaboration et caractérisation de poudres nanostructurées de MnO₂ et de polypyrrole: Application comme matériaux d'électrodes dans des dispositifs de stockage de l'énergie. Ph.D. Thesis, Chimie Physique et Chimie Analytique de Paris-Centre, Université Pierre et Marie Curie, Paris, France, 2014; p. 217.
13. Shiferaw, T. Investigation of the Interfaces of Solid Electrolyte Based Supercapacitors and Batteries. Ph.D. Thesis, Technischen Fakultät der Christian-Albrechts, Universität zu Kiel, Kiel, Germany, 2008.
14. Mohd Abdah, M.A.A.; Azman, N.H.N.; Kulandaivalu, S.; Sulaiman, Y. Review of the use of transition-metal-oxide and conducting polymer-based fibres for high-performance supercapacitors. *Mater. Des.* **2020**, *186*, 108199. [[CrossRef](#)]
15. Olabi, A.G.; Abbas, Q.; Abdelkareem, M.A.; Alami, A.H.; Mirzaeian, M.; Sayed, E.T. Carbon-Based Materials for Supercapacitors: Recent Progress, Challenges and Barriers. *Batteries* **2023**, *9*, 19. [[CrossRef](#)]
16. Gao, Q. Optimizing Carbon/Carbon Supercapacitors in Aqueous and Organic Electrolytes. Ph.D. Thesis, Energie, Matériaux, Sciences De la Terre et de l'Univers, Université d'Orleans, Orléans, France, 2013.
17. Segalini, J. Etude de L'adsorption des Ions dans des Carbones Microporeux; Application aux Supercondensateurs. Ph.D. Thesis, Sciences de la Matière Université de Toulouse, Toulouse, France, 2012.
18. Zhang, L.L. Carbon-Based Materials as Supercapacitor Electrodes. Ph.D. Thesis, Department of Chemical and Biomolecular Engineering, National University of Singapore, Singapore, 2010.
19. Zhang, J.; Zhao, X.S. On the Configuration of Supercapacitors for Maximizing Electrochemical Performance. *ChemSusChem* **2012**, *5*, 818–841. [[CrossRef](#)] [[PubMed](#)]
20. Simon, P.; Gogotsi, Y. Charge storage mechanism in nanoporous carbons and its consequence for electrical double layer capacitors. *Philos. Trans. Ser. A Math. Phys. Eng. Sci.* **2010**, *368*, 3457–3467. [[CrossRef](#)]
21. Chen, T.; Dai, L. Carbon nanomaterials for high-performance supercapacitors. *Mater. Today* **2013**, *16*, 272–280. [[CrossRef](#)]
22. Conte, M. Supercapacitors Technical Requirements for New Applications. *Fuel Cells* **2010**, *10*, 806–818. [[CrossRef](#)]
23. Roland, G.; Hamid, G. Industrial Production of Double-Layer Capacitors. In *Carbons for Electrochemical Energy Storage and Conversion Systems*; CRC Press: Boca Raton, FL, USA, 2009; pp. 429–467. [[CrossRef](#)]
24. Lu, W.; Dai, L. *Carbon Nanotube Supercapacitors*; Mauricio, M.J., Ed.; Carbon Nanotubes; IntechOpen: Rijeka, Croatia, 2010; p. 29.
25. Béguin, F.; Presser, V.; Balducci, A.; Frackowiak, E. Carbons and Electrolytes for Advanced Supercapacitors. *Adv. Mater.* **2014**, *26*, 2219–2251. [[CrossRef](#)]
26. Candelaria, S.L.; Shao, Y.; Zhou, W.; Li, X.; Xiao, J.; Zhang, J.-G.; Wang, Y.; Liu, J.; Li, J.; Cao, G. Nanostructured carbon for energy storage and conversion. *Nano Energy* **2012**, *1*, 195–220. [[CrossRef](#)]
27. Davies, A.; Yu, A. Material advancements in supercapacitors: From activated carbon to carbon nanotube and graphene. *Can. J. Chem. Eng.* **2011**, *89*, 1342–1357. [[CrossRef](#)]
28. Come, J. Caractérisation Electrochimique de Matériaux à Insertion de Li pour Supercondensateurs Hybrides à Haute Densité D'énergie. Ph.D. Thesis, Sciences et Génie des Matériaux, Université de Toulouse, Toulouse, France, 2012.
29. Halper, M.S.E.; James, C. *Supercapacitors: A Brief Overview*; The MITRE Corporation: McLean, VA, USA, 2006.
30. Simon, P.; Gogotsi, Y. Capacitive Energy Storage in Nanostructured Carbon–Electrolyte Systems. *Acc. Chem. Res.* **2013**, *46*, 1094–1103. [[CrossRef](#)] [[PubMed](#)]
31. Zhang, L.L.; Zhao, X.S. Carbon-based materials as supercapacitor electrodes. *Chem. Soc. Rev.* **2009**, *38*, 2520–2531. [[CrossRef](#)] [[PubMed](#)]
32. Kotzabasaki, M.; Sotiropoulos, I.; Charitidis, C.; Sarimveis, H. Machine learning methods for multi-walled carbon nanotubes (MWCNT) genotoxicity prediction. *Nanoscale Adv.* **2021**, *3*, 3167–3176. [[CrossRef](#)] [[PubMed](#)]
33. Maheswaran, R.; Shanmugavel, B.P. A Critical Review of the Role of Carbon Nanotubes in the Progress of Next-Generation Electronic Applications. *J. Electron. Mater.* **2022**, *51*, 2786–2800. [[CrossRef](#)]
34. Yan, J.; Wang, Q.; Wei, T.; Fan, Z. Recent Advances in Design and Fabrication of Electrochemical Supercapacitors with High Energy Densities. *Adv. Energy Mater.* **2014**, *4*, 1300816. [[CrossRef](#)]
35. Hu, L.; Hecht, D.S.; Gruener, G. Carbon Nanotube Thin Films: Fabrication, Properties, and Applications. *Chem. Rev.* **2010**, *110*, 5790–5844. [[CrossRef](#)]

36. Szabó, A.; Perri, C.; Csató, A.; Giordano, G.; Vuono, D.; Nagy, J.B. Synthesis Methods of Carbon Nanotubes and Related Materials. *Materials* **2010**, *3*, 3092–3140. [[CrossRef](#)]
37. Baddour, C.E.; Briens, C.L.; Bordere, S.; Anglerot, D.; Gaillard, P. An investigation of carbon nanotube jet grinding. *Chem. Eng. Process. Process Intensif.* **2008**, *47*, 2195–2202. [[CrossRef](#)]
38. Eatemadi, A.; Daraee, H.; Karimkhanloo, H.; Kouhi, M.; Zarghami, N.; Akbarzadeh, A.; Abasi, M.; Hanifehpour, Y.; Joo, S.W. Carbon nanotubes: Properties, synthesis, purification, and medical applications. *Nanoscale Res. Lett.* **2014**, *9*, 393. [[CrossRef](#)] [[PubMed](#)]
39. Iijima, S. Helical microtubules of graphitic carbon. *Nature* **1991**, *354*, 56–58. [[CrossRef](#)]
40. Guo, T.; Nikolaev, P.; Thess, A.; Colbert, D.T.; Smalley, R.E. Catalytic growth of single-walled nanotubes by laser vaporization. *Chem. Phys. Lett.* **1995**, *243*, 49–54. [[CrossRef](#)]
41. José-Yacamán, M.; Miki-Yoshida, M.; Rendón, L.; Santiesteban, J.G. Catalytic growth of carbon microtubules with fullerene structure. *Appl. Phys. Lett.* **1993**, *62*, 202–204. [[CrossRef](#)]
42. Prasek, J.; Drbohlavova, J.; Chomoucka, J.; Hubalek, J.; Jasek, O.; Adam, V.; Kizek, R. Methods for carbon nanotubes synthesis—Review. *J. Mater. Chem.* **2011**, *21*, 15872. [[CrossRef](#)]
43. Cadek, M.; Vostrowsky, O.; Hirsch, A. Carbon, 7. Fullerenes and Carbon Nanomaterials. In *Ullmann's Encyclopedia of Industrial Chemistry*; Wiley: Hoboken, NJ, USA, 2010.
44. Raccichini, R.; Varzi, A.; Passerini, S.; Scrosati, B. The role of graphene for electrochemical energy storage. *Nat. Mater.* **2015**, *14*, 271–279. [[CrossRef](#)]
45. Hummers, W.S.; Offeman, R.E. Preparation of Graphitic Oxide. *J. Am. Chem. Soc.* **1958**, *80*, 1339. [[CrossRef](#)]
46. Dreyer, D.R.; Park, S.; Bielawski, C.W.; Ruoff, R.S. The chemistry of graphene oxide. *Chem. Soc. Rev.* **2010**, *39*, 228–240. [[CrossRef](#)] [[PubMed](#)]
47. Sengupta, I.; Chakraborty, S.; Talukdar, M.; Pal, S.K.; Chakraborty, S. Thermal reduction of graphene oxide: How temperature influences purity. *J. Mater. Res.* **2018**, *33*, 4113–4122. [[CrossRef](#)]
48. Botas, C.; Álvarez, P.; Blanco, C.; Santamaría, R.; Granda, M.; Gutiérrez, M.D.; Rodríguez-Reinoso, F.; Menéndez, R. Critical temperatures in the synthesis of graphene-like materials by thermal exfoliation–reduction of graphite oxide. *Carbon* **2013**, *52*, 476–485. [[CrossRef](#)]
49. Hung, Y.-F.; Cheng, C.; Huang, C.-K.; Yang, C.-R. A Facile Method for Batch Preparation of Electrochemically Reduced Graphene Oxide. *Nanomaterials* **2019**, *9*, 376. [[CrossRef](#)] [[PubMed](#)]
50. Goubaa, H.; Escobar-Teran, F.; Ressay, I.; Gao, W.; El Kadib, A.; Lucas, I.T.; Raihane, M.; Lahcini, M.; Perrot, H.; Sel, O. Dynamic Resolution of Ion Transfer in Electrochemically Reduced Graphene Oxides Revealed by Electrogravimetric Impedance. *J. Phys. Chem. C* **2017**, *121*, 9370–9380. [[CrossRef](#)]
51. Inagaki, M.; Konno, H.; Tanaike, O. Carbon materials for electrochemical capacitors. *J. Power Sources* **2010**, *195*, 7880–7903. [[CrossRef](#)]
52. Lazzari, M. Electrode Materials for Ionic Liquid Based-Supercapacitors. Ph.D. Thesis, CHIM/02, CHIM/03. Università di Bologna, Bologna, Italy, 2010.
53. Salitra, G.; Soffer, A.; Eliad, L.; Cohen, Y.; Aurbach, D. Carbon Electrodes for Double-Layer Capacitors I. Relations Between Ion and Pore Dimensions. *J. Electrochem. Soc.* **2000**, *147*, 2486. [[CrossRef](#)]
54. Matsuoka, K.; Yamagishi, Y.; Yamazaki, T.; Setoyama, N.; Tomita, A.; Kyotani, T. Extremely high microporosity and sharp pore size distribution of a large surface area carbon prepared in the nanochannels of zeolite Y. *Carbon* **2005**, *43*, 876–879. [[CrossRef](#)]
55. Montes-Moran, M.A.; Suarez, D.; Menendez, J.A.; Fuente, E. On the nature of basic sites on carbon surfaces: An overview. *Carbon* **2004**, *42*, 1219–1225. [[CrossRef](#)]
56. Yoon, S.H.; Lim, S.; Song, Y.; Ota, Y.; Qiao, W.M.; Tanaka, A.; Mochida, I. KOH activation of carbon nanofibers. *Carbon* **2004**, *42*, 1723–1729. [[CrossRef](#)]
57. Vix-Guterl, C.; Frackowiak, E.; Jurewicz, K.; Friebe, M.; Parmentier, J.; Béguin, F. Electrochemical energy storage in ordered porous carbon materials. *Carbon* **2005**, *43*, 1293–1302. [[CrossRef](#)]
58. Mysyk, R.; Raymundo-Piñero, E.; Béguin, F. Saturation of subnanometer pores in an electric double-layer capacitor. *Electrochem. Commun.* **2009**, *11*, 554–556. [[CrossRef](#)]
59. Ania, C.O.; Pernak, J.; Stefaniak, F.; Raymundo-Piñero, E.; Béguin, F. Polarization-induced distortion of ions in the pores of carbon electrodes for electrochemical capacitors. *Carbon* **2009**, *47*, 3158–3166. [[CrossRef](#)]
60. Chmiola, J.; Yushin, G.; Gogotsi, Y.; Portet, C.; Simon, P.; Taberna, P.-L. Anomalous increase in carbon capacitance at pore sizes less than 1 nanometer. *Science* **2006**, *313*, 1760–1763. [[CrossRef](#)] [[PubMed](#)]
61. Faraji, S.; Ani, F.N. Microwave-assisted synthesis of metal oxide/hydroxide composite electrodes for high power supercapacitors—A review. *J. Power Sources* **2014**, *263*, 338–360. [[CrossRef](#)]
62. Carter, C.B.; Norton, M.G. Energy Production and Storage. In *Ceramic Materials*; Springer: New York, NY, USA, 2013; pp. 699–712. [[CrossRef](#)]
63. Alresheedi, B. Supercapacitors Based on Carbon Nanotube Fuzzy Fabric Structural Composites. Ph.D. Thesis, School of Engineering, University of Dayton, Dayton, OH, USA, 2012.

64. Abdisattar, A.; Yeleuov, M.; Daulbayev, C.; Askaruly, K.; Tolyzbekov, A.; Taurbekov, A.; Prikhodko, N. Recent advances and challenges of current collectors for supercapacitors. *Electrochem. Commun.* **2022**, *142*, 107373. [[CrossRef](#)]
65. Pan, H.; Li, J.; Feng, Y. Carbon Nanotubes for Supercapacitor. *Nanoscale Res. Lett.* **2010**, *5*, 654–668. [[CrossRef](#)] [[PubMed](#)]
66. Zhou, C.; Kumar, S.; Doyle, C.D.; Tour, J.M. Functionalized Single Wall Carbon Nanotubes Treated with Pyrrole for Electrochemical Supercapacitor Membranes. *Chem. Mater.* **2005**, *17*, 1997–2002. [[CrossRef](#)]
67. Zhou, Y.K.; He, B.L.; Zhou, W.J.; Li, H.L. Preparation and Electrochemistry of SWNT/PANI composite films for electrochemical capacitors. *J. Electrochem. Soc.* **2004**, *151*, A1052–A1057. [[CrossRef](#)]
68. Armand, M.; Endres, F.; MacFarlane, D.R.; Ohno, H.; Scrosati, B. Ionic-liquid materials for the electrochemical challenges of the future. *Nat. Mater.* **2009**, *8*, 621–629. [[CrossRef](#)]
69. Lin, R.; Taberna, P.-L.; Fantini, S.; Presser, V.; Pérez, C.R.; Malbosc, F.; Rupesinghe, N.L.; Teo, K.B.K.; Gogotsi, Y.; Simon, P. Capacitive Energy Storage from -50 to 100 °C Using an Ionic Liquid Electrolyte. *J. Phys. Chem. Lett.* **2011**, *2*, 2396–2401. [[CrossRef](#)]
70. Yao, F.; Pham, D.T.; Lee, Y.H. Carbon-Based Materials for Lithium-Ion Batteries, Electrochemical Capacitors, and Their Hybrid Devices. *ChemSusChem* **2015**, *8*, 2284–2311. [[CrossRef](#)]
71. Majumdar, D.; Maiyalagan, T.; Jiang, Z. Recent Progress in Ruthenium Oxide-Based Composites for Supercapacitor Applications. *ChemElectroChem* **2019**, *6*, 4343–4372. [[CrossRef](#)]
72. Arias, C.R.; Debiemme-Chouvy, C.; Gabrielli, C.; Laberty-Robert, C.; Pailleret, A.; Perrot, H.; Sel, O. New Insights into Pseudocapacitive Charge-Storage Mechanisms in Li-Birnessite Type MnO_2 Monitored by Fast Quartz Crystal Microbalance Methods. *J. Phys. Chem. C* **2014**, *118*, 26551–26559. [[CrossRef](#)]
73. Laforgue, A.; Simon, P.; Fauvarque, J.F. Chemical synthesis and characterization of fluorinated polyphenylthiophenes: Application to energy storage. *Synth. Met.* **2001**, *123*, 311–319. [[CrossRef](#)]
74. Naoi, K.; Suematsu, S.; Manago, A. Electrochemistry of poly(1,5-diaminoanthraquinone) and its application in electrochemical capacitor materials. *J. Electrochem. Soc.* **2000**, *147*, 420–426. [[CrossRef](#)]
75. Merlet, C. Modélisation de L'adsorption des Ions dans les Carbones Nanoporeux. Ph.D. Thesis, Theoretical and Physical Chemistry, Université Pierre et Marie Curie, Paris, France, 2013.
76. Odru, P. *Le Stockage de L'énergie*, 2nd ed.; Dunod: Paris, France, 2013.
77. Cao, Z.; Wei, B. A perspective: Carbon nanotube macro-films for energy storage. *Energy Environ. Sci.* **2013**, *6*, 3183–3201. [[CrossRef](#)]
78. Imani, A.; Farzi, G. Facile route for multi-walled carbon nanotube coating with polyaniline: Tubular morphology nanocomposites for supercapacitor applications. *J. Mater. Sci. Mater. Electron.* **2015**, *26*, 7438–7444. [[CrossRef](#)]
79. Zhou, Y.; Xu, H.; Lachman, N.; Ghaffari, M.; Wu, S.; Liu, Y.; Ugur, A.; Gleason, K.K.; Wardle, B.L.; Zhang, Q.M. Advanced asymmetric supercapacitor based on conducting polymer and aligned carbon nanotubes with controlled nanomorphology. *Nano Energy* **2014**, *9*, 176–185. [[CrossRef](#)]
80. Tahir, M.; He, L.; Haider, W.A.; Yang, W.; Hong, X.; Guo, Y.; Pan, X.; Tang, H.; Li, Y.; Mai, L. Co-Electrodeposited porous PEDOT–CNT microelectrodes for integrated micro-supercapacitors with high energy density, high rate capability, and long cycling life. *Nanoscale* **2019**, *11*, 7761–7770. [[CrossRef](#)]
81. Chen, Y.; Du, L.; Yang, P.; Sun, P.; Yu, X.; Mai, W. Significantly enhanced robustness and electrochemical performance of flexible carbon nanotube-based supercapacitors by electrodepositing polypyrrole. *J. Power Sources* **2015**, *287*, 68–74. [[CrossRef](#)]
82. Fu, C.; Zhou, H.; Liu, R.; Huang, Z.; Chen, J.; Kuang, Y. Supercapacitor based on electropolymerized polythiophene and multi-walled carbon nanotubes composites. *Mater. Chem. Phys.* **2012**, *132*, 596–600. [[CrossRef](#)]
83. El-Shahat, M.; Mochtar, M.; Rashad, M.M.; Mousa, M.A. Single and ternary nanocomposite electrodes of $Mn_3O_4/TiO_2/rGO$ for supercapacitors. *J. Solid State Electrochem.* **2021**, *25*, 803–819. [[CrossRef](#)]
84. Kumar, N.; Kim, S.-B.; Lee, S.-Y.; Park, S.-J. Recent Advanced Supercapacitor: A Review of Storage Mechanisms, Electrode Materials, Modification, and Perspectives. *Nanomaterials* **2022**, *12*, 3708. [[CrossRef](#)]
85. Satpathy, S.; Debbarma, S.; Kumar Bhattacharyya, B. An integration of the review of electrode's materials and a new gamma function-based charging methodology of supercapacitor for high current applications. *Mater. Today Proc.* **2020**, *26*, 2151–2156. [[CrossRef](#)]
86. Shown, I.; Ganguly, A.; Chen, L.-C.; Chen, K.-H. Conducting polymer-based flexible supercapacitor. *Energy Sci. Eng.* **2015**, *3*, 2–26. [[CrossRef](#)]
87. Lemian, D.; Bode, F. Battery-Supercapacitor Energy Storage Systems for Electrical Vehicles: A Review. *Energies* **2022**, *15*, 5683. [[CrossRef](#)]
88. Fakhry, A. Synthèse par Voie Électrochimique de Nanostructures de Polymères Conducteurs sans Emploi d'une Matrice Support. Applications Aux (bio)capteurs. Ph.D. Thesis, Université Pierre et Marie Curie, Paris, France, 2014.
89. To Thi Kim, L. Etude de Films Électroactifs par Couplage de Techniques Électrochimique et Gravimétrique. Application à la Caractérisation de Membranes à Conduction Protonique. Ph.D. Thesis, Chimie Physique et Chimie Analytique, Université Pierre et Marie Curie, Paris, France, 2009.
90. Permatasari, F.A.; Irham, M.A.; Bisri, S.Z.; Iskandar, F. Carbon-Based Quantum Dots for Supercapacitors: Recent Advances and Future Challenges. *Nanomaterials* **2021**, *11*, 91. [[CrossRef](#)]

91. Verma, S.; Pandey, V.K.; Verma, B. Synthesis and supercapacitor performance studies of graphene oxide based ternary composite. *Mater. Technol.* **2022**, *37*, 2915–2931. [[CrossRef](#)]
92. Thissandier, F. Elaboration de Micro-Supercondensateurs à Base D'électrodes en Silicium Nanostructuré: Des Nanomatériaux aux Dispositifs. Ph.D. Thesis, Chimie et Sciences du Vivant, Université de Grenoble, Grenoble, France, 2006.
93. Portet, C.; Taberna, P.L.; Simon, P.; Flahaut, E.; Laberty-Robert, C. High power density electrodes for Carbon supercapacitor applications. *Electrochim. Acta* **2005**, *50*, 4174–4181. [[CrossRef](#)]
94. Pacios Pujadó, M. Introduction. In *Carbon Nanotubes as Platforms for Biosensors with Electrochemical and Electronic Transduction*; Springer: Berlin/Heidelberg, Germany, 2012; pp. 1–78. [[CrossRef](#)]
95. Portet, C.; Taberna, P.L.; Simon, P.; Flahaut, E. Influence of carbon nanotubes addition on carbon-carbon supercapacitor performances in organic electrolyte. *J. Power Sources* **2005**, *139*, 371–378. [[CrossRef](#)]
96. Rajasekaran, S.J.; Grace, A.N.; Jacob, G.; Alodhayb, A.; Pandiaraj, S.; Raghavan, V. Investigation of Different Aqueous Electrolytes for Biomass-Derived Activated Carbon-Based Supercapacitors. *Catalysts* **2023**, *13*, 286. [[CrossRef](#)]
97. Escobar-Teran, F.; Perrot, H.; Sel, O. Ion Dynamics at the Single Wall Carbon Nanotube Based Composite Electrode/Electrolyte Interface: Influence of the Cation Size and the Electrolyte pH. *J. Phys. Chem. C* **2019**, *123*, 4262–4273. [[CrossRef](#)]
98. Inzelt, G. Electrochemical Quartz Crystal Nanobalance. In *Electroanalytical Methods*; Scholz, F., Bond, A.M., Compton, R.G., Fiedler, D.A., Inzelt, G., Kahlert, H., Komorsky-Lovrić, Š., Lohse, H., Lovrić, M., Marken, F., et al., Eds.; Springer: Berlin/Heidelberg, Germany, 2010; pp. 257–270. [[CrossRef](#)]
99. Sigalov, S.; Levi, M.D.; Daikhin, L.; Salitra, G.; Aurbach, D. Electrochemical quartz crystal admittance studies of ion adsorption on nanoporous composite carbon electrodes in aprotic solutions. *J. Solid State Electrochem.* **2013**, *18*, 1335–1344. [[CrossRef](#)]
100. Sel, O.; Kim, L.T.T.; Debiemme-Chouvy, C.; Gabrielli, C.; Laberty-Robert, C.; Perrot, H.; Sanchez, C. Proton Insertion Properties in a Hybrid Membrane/Conducting Polymer Bilayer Investigated by AC Electrogravimetry. *J. Electrochem. Soc.* **2010**, *157*, F69. [[CrossRef](#)]
101. Agrisuelas, J. Síntesis y Caracterización de Polímeros Electroactivos en Sistemas Multicapa. Ph.D. Thesis, Química Física, Universitat de Valencia, València, Spain, 2008.
102. Bruckenstein, S.; Swathirajan, S. Potential dependence of lead and silver underpotential coverages in acetonitrile using a piezoelectric crystal oscillator method. *Electrochim. Acta* **1985**, *30*, 851–855. [[CrossRef](#)]
103. Hepel, M.; Bruckenstein, S. Tracking anion expulsion during underpotential deposition of lead at silver using the quartz microbalance. *Electrochim. Acta* **1989**, *34*, 1499–1504. [[CrossRef](#)]
104. Hepel, M.; Kanige, K.; Bruckenstein, S. In situ underpotential deposition study of lead on silver using the electrochemical quartz crystal microbalance: Direct evidence for lead(II) adsorption before spontaneous charge transfer. *J. Electroanal. Chem. Interfacial Electrochem.* **1989**, *266*, 409–421. [[CrossRef](#)]
105. Schumacher, R.; Borges, G.; Kanazawa, K.K. The quartz microbalance: A sensitive tool to probe surface reconstructions on gold electrodes in liquid. *Surf. Sci.* **1985**, *163*, L621–L626. [[CrossRef](#)]
106. Ostrom, G.S.; Buttry, D.A. Quartz crystal microbalance studies of deposition and dissolution mechanisms of electrochromic films of diheptylviologen bromide. *J. Electroanal. Chem. Interfacial Electrochem.* **1988**, *256*, 411–431. [[CrossRef](#)]
107. Levi, M.D.; Sigalov, S.; Aurbach, D.; Daikhin, L. In Situ Electrochemical Quartz Crystal Admittance Methodology for Tracking Compositional and Mechanical Changes in Porous Carbon Electrodes. *J. Phys. Chem. C* **2013**, *117*, 14876–14889. [[CrossRef](#)]
108. Sigalov, S.; Levi, M.D.; Salitra, G.; Aurbach, D.; Jänes, A.; Lust, E.; Halalay, I.C. Selective adsorption of multivalent ions into TiC-derived nanoporous carbon. *Carbon* **2012**, *50*, 3957–3960. [[CrossRef](#)]
109. Sigalov, S.; Levi, M.D.; Salitra, G.; Aurbach, D.; Maier, J. EQCM as a unique tool for determination of ionic fluxes in microporous carbons as a function of surface charge distribution. *Electrochem. Commun.* **2010**, *12*, 1718–1721. [[CrossRef](#)]
110. Tsai, W.-Y.; Taberna, P.-L.; Simon, P. Electrochemical Quartz Crystal Microbalance (EQCM) Study of Ion Dynamics in Nanoporous Carbons. *J. Am. Chem. Soc.* **2014**, *136*, 8722–8728. [[CrossRef](#)]
111. Dargel, V.; Shpigel, N.; Sigalov, S.; Nayak, P.; Levi, M.D.; Daikhin, L.; Aurbach, D. In situ real-time gravimetric and viscoelastic probing of surface films formation on lithium batteries electrodes. *Nat Commun* **2017**, *8*, 1389. [[CrossRef](#)] [[PubMed](#)]
112. Shpigel, N.; Levi, M.D.; Aurbach, D. EQCM-D technique for complex mechanical characterization of energy storage electrodes: Background and practical guide. *Energy Storage Mater.* **2019**, *21*, 399–413. [[CrossRef](#)]
113. Malka, D.; Attias, R.; Shpigel, N.; Malchick, F.; Levi, M.D.; Aurbach, D. Horizons for Modern Electrochemistry Related to Energy Storage and Conversion, a Review. *Isr. J. Chem.* **2021**, *61*, 11–25. [[CrossRef](#)]
114. Shpigel, N.; Chakraborty, A.; Malchik, F.; Bergman, G.; Nimkar, A.; Gavriel, B.; Turgeman, M.; Hong, C.N.; Lukatskaya, M.R.; Levi, M.D.; et al. Can Anions Be Inserted into MXene? *J. Am. Chem. Soc.* **2021**, *143*, 12552–12559. [[CrossRef](#)]
115. Lin, Z.; Taberna, P.-L.; Simon, P. Electrochemical double layer capacitors: What is next beyond the corner? *Curr. Opin. Electrochem.* **2017**, *6*, 115–119. [[CrossRef](#)]
116. Barisci, J.N.; Wallace, G.G.; Baughman, R.H. Electrochemical quartz crystal microbalance studies of single-wall carbon nanotubes in aqueous and non-aqueous solutions. *Electrochim. Acta* **2000**, *46*, 509–517. [[CrossRef](#)]

117. Levi, M.D.; Salitra, G.; Levy, N.; Aurbach, D.; Maier, J. Application of a quartz-crystal microbalance to measure ionic fluxes in microporous carbons for energy storage. *Nat. Mater.* **2009**, *8*, 872–875. [[CrossRef](#)] [[PubMed](#)]
118. Levi, M.D.; Sigalov, S.; Salitra, G.; Aurbach, D.; Maier, J. The effect of specific adsorption of cations and their size on the charge-compensation mechanism in carbon micropores: The role of anion desorption. *Chemphyschem* **2011**, *12*, 854–862. [[CrossRef](#)] [[PubMed](#)]
119. Escobar-Teran, F.; Arnau, A.; Garcia, J.V.; Jiménez, Y.; Perrot, H.; Sel, O. Gravimetric and dynamic deconvolution of global EQCM response of carbon nanotube based electrodes by Ac-electrogravimetry. *Electrochem. Commun.* **2016**, *70*, 73–77. [[CrossRef](#)]
120. Bourkane, S.; Gabrielli, C.; Keddam, M. Investigation of gold oxidation in sulphuric medium—II. Electrogravimetric transfer function technique. *Electrochim. Acta* **1993**, *38*, 1827–1835. [[CrossRef](#)]
121. Bourkane, S.; Gabrielli, C.; Keddam, M. Kinetic study of electrode processes by ac quartz electrogravimetry. *J. Electroanal. Chem. Interfacial Electrochem.* **1988**, *256*, 471–475. [[CrossRef](#)]
122. Halim, E.M.; Demir-Cakan, R.; Perrot, H.; El Rhazi, M.; Sel, O. Interfacial charge storage mechanisms of composite electrodes based on poly(ortho-phenylenediamine)/carbon nanotubes via advanced electrogravimetry. *J. Chem. Phys.* **2022**, *156*, 124703. [[CrossRef](#)]
123. Forse, A.C.; Griffin, J.M.; Grey, C.P. Selective observation of charge storing ions in supercapacitor electrode materials. *Solid State Nucl. Magn. Reson.* **2018**, *89*, 45–49. [[CrossRef](#)] [[PubMed](#)]
124. Forse, A.C.; Griffin, J.M.; Merlet, C.; Carretero-Gonzalez, J.; Raji, A.-R.O.; Trease, N.M.; Grey, C.P. Direct observation of ion dynamics in supercapacitor electrodes using in situ diffusion NMR spectroscopy. *Nat. Energy* **2017**, *2*, 16216. [[CrossRef](#)]
125. Forse, A.C.; Merlet, C.; Griffin, J.M.; Grey, C.P. New Perspectives on the Charging Mechanisms of Supercapacitors. *J. Am. Chem. Soc.* **2016**, *138*, 5731–5744. [[CrossRef](#)] [[PubMed](#)]
126. Griffin, J.M.; Forse, A.C.; Grey, C.P. Solid-state NMR studies of supercapacitors. *Solid State Nucl. Magn. Reson.* **2016**, *74–75*, 16–35. [[CrossRef](#)]
127. Griffin, J.M.; Forse, A.C.; Tsai, W.-Y.; Taberna, P.-L.; Simon, P.; Grey, C.P. In situ NMR and electrochemical quartz crystal microbalance techniques reveal the structure of the electrical double layer in supercapacitors. *Nat. Mater.* **2015**, *14*, 812–819. [[CrossRef](#)]
128. Forse, A.C.; Merlet, C.; Allan, P.K.; Humphreys, E.K.; Griffin, J.M.; Aslan, M.; Zeiger, M.; Presser, V.; Gogotsi, Y.; Grey, C.P. New Insights into the Structure of Nanoporous Carbons from NMR, Raman, and Pair Distribution Function Analysis. *Chem. Mater.* **2015**, *27*, 6848–6857. [[CrossRef](#)]
129. Forse, A.C.; Griffin, J.M.; Merlet, C.; Bayley, P.M.; Wang, H.; Simon, P.; Grey, C.P. NMR Study of Ion Dynamics and Charge Storage in Ionic Liquid Supercapacitors. *J. Am. Chem. Soc.* **2015**, *137*, 7231–7242. [[CrossRef](#)] [[PubMed](#)]
130. Griffin, J.M.; Forse, A.C.; Wang, H.; Trease, N.M.; Taberna, P.-L.; Simon, P.; Grey, C.P. Ion counting in supercapacitor electrodes using NMR spectroscopy. *Faraday Discuss.* **2014**, *176*, 49–68. [[CrossRef](#)]
131. Coretti, A.; Bacon, C.; Berthin, R.; Serva, A.; Scalfi, L.; Chubak, I.; Goloviznina, K.; Haefele, M.; Marin-Laflèche, A.; Rotenberg, B.; et al. MetalWalls: Simulating electrochemical interfaces between polarizable electrolytes and metallic electrodes. *J. Chem. Phys.* **2022**, *157*, 184801. [[CrossRef](#)]
132. Scalfi, L.; Salanne, M.; Rotenberg, B. Molecular Simulation of Electrode-Solution Interfaces. *Annu. Rev. Phys. Chem.* **2021**, *72*, 189–212. [[CrossRef](#)] [[PubMed](#)]
133. Jeanmairat, G.; Rotenberg, B.; Salanne, M. Microscopic Simulations of Electrochemical Double-Layer Capacitors. *Chem. Rev.* **2022**, *122*, 10860–10898. [[CrossRef](#)] [[PubMed](#)]
134. Salanne, M.; Rotenberg, B.; Naoi, K.; Kaneko, K.; Taberna, P.L.; Grey, C.P.; Dunn, B.; Simon, P. Efficient storage mechanisms for building better supercapacitors. *Nat. Energy* **2016**, *1*, 16070. [[CrossRef](#)]
135. Zou, Z.; Liu, L.; Meng, S.; Bian, X.; Li, Y. Applicability of Different Double-Layer Models for the Performance Assessment of the Capacitive Energy Extraction Based on Double Layer Expansion (CDLE) Technique. *Energies* **2021**, *14*, 5828. [[CrossRef](#)]
136. Li, Z.; Mendez-Morales, T.; Salanne, M. Computer simulation studies of nanoporous carbon-based electrochemical capacitors. *Curr. Opin. Electrochem.* **2018**, *9*, 81–86. [[CrossRef](#)]
137. Bo, Z.; Li, C.; Yang, H.; Ostrikov, K.; Yan, J.; Cen, K. Design of Supercapacitor Electrodes Using Molecular Dynamics Simulations. *Nano-Micro Lett.* **2018**, *10*, 33. [[CrossRef](#)]
138. Fedorov, M.V.; Kornyshev, A.A. Ionic Liquids at Electrified Interfaces. *Chem. Rev.* **2014**, *114*, 2978–3036. [[CrossRef](#)]
139. Landers, J.; Gor, G.Y.; Neimark, A.V. Density functional theory methods for characterization of porous materials. *Colloids Surf. A Physicochem. Eng. Asp.* **2013**, *437*, 3–32. [[CrossRef](#)]
140. Xu, K.; Shao, H.; Lin, Z.; Merlet, C.; Feng, G.; Zhu, J.; Simon, P. Computational Insights into Charge Storage Mechanisms of Supercapacitors. *Energy Environ. Mater.* **2020**, *3*, 235–246. [[CrossRef](#)]
141. Huang, J.; Sumpter, B.G.; Meunier, V. Theoretical Model for Nanoporous Carbon Supercapacitors. *Angew. Chem. Int. Ed.* **2008**, *47*, 520–524. [[CrossRef](#)] [[PubMed](#)]
142. Huang, J.; Sumpter, B.G.; Meunier, V. A universal model for nanoporous carbon supercapacitors applicable to diverse pore regimes, carbon materials, and electrolytes. *Chem.-A Eur. J.* **2008**, *14*, 6614–6626. [[CrossRef](#)] [[PubMed](#)]
143. Kalluri, R.K.; Konatham, D.; Striolo, A. Aqueous NaCl Solutions within Charged Carbon-Slit Pores: Partition Coefficients and Density Distributions from Molecular Dynamics Simulations. *J. Phys. Chem. C* **2011**, *115*, 13786–13795. [[CrossRef](#)]

144. Merlet, C.; Péan, C.; Rotenberg, B.; Madden, P.A.; Daffos, B.; Taberna, P.L.; Simon, P.; Salanne, M. Highly confined ions store charge more efficiently in supercapacitors. *Nat. Commun.* **2013**, *4*, 2701. [[CrossRef](#)]
145. Prehal, C.; Koczwara, C.; Jäckel, N.; Schreiber, A.; Burian, M.; Amenitsch, H.; Hartmann, M.A.; Presser, V.; Paris, O. Quantification of ion confinement and desolvation in nanoporous carbon supercapacitors with modelling and in situ X-ray scattering. *Nat. Energy* **2017**, *2*, 16215. [[CrossRef](#)]

Disclaimer/Publisher's Note: The statements, opinions and data contained in all publications are solely those of the individual author(s) and contributor(s) and not of MDPI and/or the editor(s). MDPI and/or the editor(s) disclaim responsibility for any injury to people or property resulting from any ideas, methods, instructions or products referred to in the content.